Pyruvate-formate lyase–derived formate regulates the response of *Salmonella* Typhimurium to meropenem and ciprofloxacin.

Short title: Formate shapes response of *Salmonella* to meropenem and ciprofloxacin

Debapriya Mukherjee[1], Sakshi Vasant Wagle[1#], Pallab Ghosh[1#], Abhishek Biswas[1], Dipshikha Chakravortty[1,2*]

[1]Department of Microbiology and Cell Biology, Division of Biological Sciences, Indian Institute of Science, Bangalore, India.

[2]School of Biology, Indian Institute of Science Education and Research, Thiruvananthapuram, 695551.

#Equal contribution

[*]Corresponding author: dipa@iisc.ac.in

Tel: 0091 80 2293 2842

Fax: 0091 80 2360 2697

Abstract

Salmonella enterica serovar Typhimurium (STM) employs various strategies to endure antibiotic stress, but the contribution of central metabolites to resistance remains insufficiently characterized. In this work, we identify intracellular formate, produced by pyruvate-formate lyase (PflB), as a key determinant of STM susceptibility to meropenem and ciprofloxacin. Deletion of *pflB* disrupts cellular pH homeostasis, impairing efflux pump function, increasing reactive oxygen species, and causing membrane depolarization, collectively heightening sensitivity to antibiotics. Supplementing extracellular formate reverses these phenotypes. Mechanistically, pH imbalance activates the RpoE–*csrB* regulatory pathway, leading to reduced expression of efflux pump genes *acrB* and *tolC*, while extracellular formate engages the BarA/SirA two-component system to further influence the CsrA/*csrB* network. Disrupting the formate pool interferes with efflux-dependent resistance, revealing a previously unrecognized signalling function for intracellular metabolites. Overall, our results position formate as a metabolic driver of antibiotic outcomes in STM and highlight it as a potential target for mitigating resistance.

Keywords: PflB, Antimicrobial response (AMR), Efflux pumps, CsrA/*csrB* axis

46 # Introduction

47 The global escalation of antimicrobial resistance (AMR) has been driven largely by decades of
48 antibiotic overuse and misuse (1, 2). Among the resistant pathogens of greatest concern,
49 multidrug-resistant (MDR) *Salmonella* has become a significant public health threat,
50 contributing heavily to global illness and death. In 2019, AMR-associated *Salmonella*
51 infections were estimated to cause approximately 150,000 deaths worldwide, with 23,700 of
52 these attributed specifically to MDR strains (3). Within this landscape, *Salmonella enterica*
53 serovar Typhimurium (STM) remains one of the most prevalent MDR serotypes,
54 compromising the efficacy of frontline antibiotics and posing major challenges to healthcare
55 systems (4-7).

56 To survive antibiotic exposure, *Salmonella* relies on a broad array of resistance mechanisms,
57 including enzymatic degradation of antimicrobial compounds, efflux pump–mediated drug
58 export, structural modification of antibiotics, and alteration or protection of cellular targets (8,
59 9). Although these classical pathways are well characterized, the influence of bacterial
60 metabolism on shaping AMR in *Salmonella* is still poorly defined.

61 Our previous work identified pyruvate-formate lyase (PflB), encoded by *pflB*, as an important
62 contributor to STM pathogenesis. PflB regulates intracellular formate levels, a short-chain fatty
63 acid essential for maintaining intracellular pH (ipH) homeostasis. Deletion of *pflB* disturbs ipH
64 balance, resulting in membrane stress, activation of the extra cytoplasmic sigma factor RpoE,
65 increased expression of the small RNA *csrB*, and repression of flagellar gene expression (10).
66 We also observed that *pflB* loss increases STM sensitivity to meropenem and ciprofloxacin,
67 pointing to a previously unrecognized relationship between formate metabolism and antibiotic
68 resistance.

69 In the present study, we systematically evaluated how intracellular formate pools and
70 extracellular formate supplementation influence antibiotic susceptibility in STM. We show that
71 the absence of *pflB* leads to disrupted internal pH, causing membrane damage that activates
72 RpoE and alters expression of the efflux pump gene *acrB*. Additionally, extracellular formate
73 modulates antibiotic resistance through the BarA/SirA two-component system and the
74 downstream CsrA/*csrB* regulatory network, collectively contributing to reduced *acrB*
75 expression. Together, these results demonstrate that intracellular formate directly governs STM
76 antibiotic susceptibility, while extracellular formate exerts distinct signalling effects. Overall,
77 our findings establish formate as a key metabolic determinant of AMR and highlight formate
78 homeostasis as a promising target for combating MDR *Salmonella*.

79

80 Materials and Methods

81 Bacterial strains and culture conditions

82 The wild-type *Salmonella enterica* subsp. *enterica* serovar Typhimurium strain 14028S used
83 in this study was kindly provided by Professor Michael Hensel (Max von Pettenkofer Institute
84 for Hygiene and Medical Microbiology, Germany). All bacterial strains were preserved as
85 glycerol stocks at −80 °C and revived on Luria-Bertani (LB) agar plates (HiMedia)
86 supplemented with the appropriate antibiotics when necessary (50 µg/ml kanamycin, 50 µg/ml
87 ampicillin, or 25 µg/ml chloramphenicol). Single colonies were inoculated into LB broth
88 supplemented with the appropriate antibiotics and incubated overnight at 37 °C with shaking
89 at 170 rpm. The overnight cultures were then diluted 1:100 in fresh LB medium, with or without
90 40 mM sodium formate (Sigma), and grown under the same conditions for 6 hours to obtain
91 bacteria in the logarithmic growth phase. The optical density at 600 nm (OD_{600}) was
92 subsequently adjusted to 0.1 in Mueller-Hinton Broth (MHB), corresponding to approximately

93 10^6 colony-forming units (CFU), for use in downstream experiments. A detailed list of bacterial

94 strains and plasmids used in this study is provided in Table 1.

95 **Table 1**

Bacterial strains/plasmids	**Characteristics**	**Source**
Salmonella enterica subspecies *enterica* serovar Typhimurium strain 14028S	Wild type	Gift from Prof. M. Hensel
STM Δ*pflB*	Kan^R	Laboratory stock
STM Δ*pflB*/pQE60*: pflB*	Kan^R, Amp^R	Laboratory stock
STM Δ*fliC*	Kan^R	Laboratory stock
STM Δ*rpoE*	Chl^R	Laboratory stock
STM Δ*pflB*Δ*rpoE*	Kan^R, Chl^R	Laboratory stock
STM Δ*sirA*	Chl^R	Laboratory stock
STM Δ*pflB*Δ*sirA*	Kan^R, Chl^R	Laboratory stock
pQE60	Low copy number plasmid, Amp^R	Laboratory stock
Cip-R C1	Ciprofloxacin resistant mutant	Laboratory stock
Cip-R C2	Ciprofloxacin resistant mutant	Laboratory stock
Cip-R C3	Ciprofloxacin resistant mutant	Laboratory stock
Mer-R C1	Meropenem resistant mutant	Laboratory stock

Mer-R C2	Meropenem resistant mutant	Laboratory stock
Mer-R C3	Meropenem resistant mutant	Laboratory stock
pQE60: *pflB*	Ampicillin resistant	Laboratory stock

96

97 **Determination of MIC of meropenem, ciprofloxacin, ceftazidime**

98 Logarithmic phase bacterial cultures, adjusted to an OD_{600} of 0.1, were inoculated into 96-well
99 microtiter plates containing Mueller-Hinton Broth (MHB) supplemented with serial dilutions
100 of antibiotics. The concentrations used were as follows: meropenem (8 to 0.0156 mg/L)
101 (Sigma), ciprofloxacin (0.5 to 0.0009 mg/L) (Sigma), and ceftazidime (128 to 0.125 mg/L).
102 Plates were incubated at 37 °C with shaking at 170 rpm for 14-16 hours. Bacterial growth was
103 assessed by measuring OD_{600} using a Tecan microplate reader.

104

105 **Estimation of bacterial viability using resazurin assay**

106 Following antibiotic exposure and incubation for 14-16 hours, 20 µL of resazurin solution
107 (prepared from a 0.2 mg/mL stock) was added to each well and incubated for 2 hours in the
108 dark. Thereafter, fluorescence intensity was measured using a Tecan microplate reader with
109 excitation at 540 nm and emission at 590 nm. Cell viability was assessed by monitoring the
110 color change of resazurin. A stronger purple coloration indicated higher cell viability.

111

112 **Flow cytometry mediated quantification of live/dead population, intracellular reactive**
113 **oxygen species (ROS), membrane depolarization, and ipH**

114 After 14–16 hours of antibiotic treatment, bacterial cells were stained with a panel of
115 fluorescent dyes: Propidium Iodide (PI, 1 μg/mL) for live/dead discrimination,
116 dichlorodihydrofluorescein diacetate (DCF_2DA, 10 μM) to assess intracellular reactive oxygen
117 species (ROS), Bis-(1,3-Dibutylbarbituric Acid) Trimethine Oxonol ($DiBAC_4$, 1 μg/mL) for
118 measuring membrane depolarization, and 2′,7′-Bis-(2-Carboxyethyl)-5-(and-6)-
119 Carboxyfluorescein Acetoxymethyl Ester (BCECF-AM, 20 μM) for intracellular pH (ipH)
120 comparison. Stained samples were incubated in the dark for 15 minutes and subsequently
121 analyzed using the BD FACSVerse flow cytometer (BD Biosciences, USA). Data including dot
122 plots, density plots, median fluorescence intensity (MFI), and the percentage of positively
123 stained cells were acquired and processed using BD FACSVerse software.
124

125 **Determination of intracellular formate and pyruvate concentration**

126 Following exposure of logarithmic-phase cultures of STM WT and passaged strains to sub-
127 lethal antibiotic concentrations and a 16-hour incubation, the cultures were centrifuged at 6,000
128 rpm for 10 minutes. The resulting pellet was washed twice with 1X PBS to remove residual
129 media and then resuspended in PBS. A 100 μl portion of this suspension was plated on LB agar
130 to determine the CFU count. The remaining suspension was lysed by sonication, and cellular
131 debris were cleared by centrifugation at 12,000 g for 10 minutes. Formate and pyruvate levels
132 in the supernatant were quantified using the Abcam formate estimation kit (ab111748) and
133 Elabscience pyruvate estimation kit (E-BC-K130-S) according to the manufacturer's
134 instructions, and the concentrations were interpolated from a standard curve. The
135 concentrations were normalized with the CFU obtained from plating.
136

137 **RNA isolation and RT-qPCR**

138 Logarithmic-phase bacterial cultures were harvested by centrifugation at 6,000 rpm for 10
139 minutes at 4 °C, and the resulting cell pellets were resuspended in TRIzol reagent. Samples
140 were stored at −80 °C until further processing. Total RNA was extracted using the chloroform–
141 isopropanol method, and RNA pellets were washed with 70% ethanol and resuspended in 30 μL
142 of DEPC-treated Milli-Q water. RNA concentration was measured using a NanoDrop
143 spectrophotometer (Thermo Fisher Scientific), and RNA integrity was verified by
144 electrophoresis on a 2% agarose gel. For removal of genomic DNA, 2 μg of total RNA was
145 treated with TURBO DNase (Thermo Fisher Scientific) at 37 °C for 30 minutes, followed by
146 inactivation with 5 mM Na_2EDTA at 65 °C for 10 minutes. First-strand cDNA synthesis was
147 performed using the PrimeScript RT reagent kit (Takara, Cat. No. RR037A) according to the
148 manufacturer's protocol. Quantitative real-time PCR (qRT-PCR) was carried out using the TB
149 Green RT-qPCR kit (Takara) on a QuantStudio 5 Real-Time PCR System. Gene expression was
150 analysed using intragenic primers and normalized to *16S rRNA* levels. Primer sequences are
151 provided in Table 2.

152 **Table 2**

Primer name	**Sequence (5'-3')**
16S *rRNA* RT FP	GTGAGGTAACGGCTCACCAA
16S *rRNA* RT RP	TAACCGCAACACCTTCCTCC
acrB RT FP	CTCTATCACCATCGTATCGG
acrB RT RP	AGTAATCCGTGACCTCATCC
tolC RT FP	TAACGAAGCGCGTAGTCCTT
tolC RT FP	AGCACATCAATAGCGTTCA
ompF RT FP	TGAATCCTATACCGATATGG
ompF RT RP	CCTGCTGATCGTTAGTACGC
emrB RT FP	TGGCGTATCCAGCAGCCTGA

emrB RT RP	GATGCCAATCACCAGTAGCG

153

154

155 **Efflux pump activity by Nile Red Assay**

156 Efflux pump activity was quantified following the method outlined by Lyu *et al*(11). In brief,
157 bacterial cultures in the logarithmic growth phase were adjusted to an optical density of 0.1 at
158 600 nm (OD_{600}). A volume of 100 µl from each normalized culture was dispensed into wells of
159 a 96-well microplate and incubated with Nile Red dye at a final concentration of 48 µg/ml. The
160 plate was incubated in the dark under shaking conditions for 3 hours. Fluorescence
161 measurements were then obtained using a TECAN microplate reader, with excitation and
162 emission wavelengths set at 549 nm and 628 nm, respectively. Fluorescence intensity values
163 were normalized against absorbance readings at 600 nm.

164

165 **Atomic Force Microscopy**

166 After 14–16 hours of antibiotic exposure, bacterial cells were drop-cast onto sterile glass
167 coverslips. Once air-dried, the cells were fixed by treating them with 3.5% paraformaldehyde
168 for 10 minutes. Residual salts were removed by washing the samples three times with double-
169 autoclaved MilliQ water. The coverslips were then dried in a vacuum desiccator prior to
170 imaging with the NX10 Atomic Force Microscope (AFM). Image processing and
171 measurements of cell length and height were performed using XEI software.

172

173 **Animal experiments**

174 All animal experiments were conducted with prior approval from the Institutional Animal
175 Ethics Clearance Committee (IAEC) at the Indian Institute of Science, Bangalore. The institute
176 is registered under CPCSEA with registration number 48/1999/CPCSEA. All procedures

177 strictly adhered to the guidelines set by the Committee for the Purpose of Control and
178 Supervision of Experiments on Animals (CPCSEA). The ethical approval number for this study
179 is CAF/Ethics/853/2021.
180 A modified protocol based on the method described by Roy Chowdhury *et al.* was employed
181 to evaluate the organ burden following infection and antibiotic treatment with the wild-type
182 (WT) and mutant bacterial strains(12). Briefly, 10^6 cells from overnight cultures were orally
183 gavaged into 6–8-week-old C57BL/6 mice on day 0 (0 dpi). Mice received 1 mg/kg of the
184 respective antibiotics on days 2 and 4 post-infection. On day 5 post-infection, the animals were
185 ethically euthanized, and the intestine, liver, and spleen were collected. These organs were
186 homogenized, and serial dilutions of the homogenates were plated on *Salmonella-Shigella* (SS)
187 agar. Bacterial load was quantified and expressed as $\log_{10}$ CFU per gram of tissue.

188 To compare mortality rates between STM WT and STM Δ*pflB* under antibiotic exposure,
189 groups of mice (n=5) were orally administered 10^6 cells from stationary phase cultures of each
190 strain. Starting from day 2 post-infection, 1 mg/kg of the respective antibiotics was
191 administered every alternate day till the mice survived. Survival was monitored daily and
192 represented as percent survival. A 125 mM solution of sodium formate was supplemented in
193 the drinking water provided to the animals in both experimental setups.

194

195 **Estimation of Formate in mouse serum by Gas Chromatography-Mass Spectrometry**

196 To quantify formate levels in mouse serum following supplementation with 125 mM sodium
197 formate in drinking water, a protocol adapted from Hughes *et al* was employed(13). Male
198 C57BL/6 mice (6–8 weeks old) were provided with 125 mM sodium formate in their drinking
199 water. At five days post-infection, blood was collected via retro-orbital puncture. After clotting,

200 serum was separated by centrifugation at 10,000 × g for 20 minutes and subsequently used for
201 formate quantification.

202 Sodium formate (Sigma) served as an external standard. Both standards and biological samples
203 were derivatized prior to mass spectrometry analysis. To protonate the formate, 2 M
204 hydrochloric acid was added to each sample in a 1:1 ratio. Liquid-liquid extraction was
205 performed to isolate formic acid into ethyl acetate (Sigma-Aldrich). Residual water was
206 removed by passing the ethyl acetate extract through an anhydrous sodium sulfate column
207 (Sigma-Aldrich). The extract was then incubated at 80 °C for 1 hour with the derivatizing
208 reagent N,O-Bis(trimethylsilyl)trifluoroacetamide (Sigma-Aldrich) containing 1%
209 chlorotrimethylsilane (Fluka). Derivatized samples were transferred to autosampler vials for
210 analysis using Gas Chromatography-Mass Spectrometry (GC-MS; Agilent Technologies,
211 7890A GC, 5975C MS).

212 Injection parameters were as follows: injection temperature of 200 °C, injection split ratio of
213 1:40, and injection volume of 1 µL. The oven temperature program began at 40 °C (held for 4
214 minutes), increased to 120 °C at a rate of 5 °C/min, and then to 200 °C at 25 °C/min, with a
215 final hold of 3 minutes. Helium was used as the carrier gas at a constant flow rate of
216 1.2 mL/min. Chromatographic separation was performed using a 30 m × 0.25 mm × 0.40 µm
217 DB-624 column (Agilent). The interface temperature was maintained at 220 °C, and the
218 electron impact ion source operated at 230 °C with an ionization energy of 70 eV and 1235 EM
219 volts.

220 For qualitative analysis, selected ion monitoring in single quadrupole mode was employed with
221 a scan at m/z 103. The retention time for formate and its deuterated analog was approximately
222 5.9 minutes. The target and reference (qualifier) ions for formate were m/z = 103 and m/z =

223 75, respectively. Sample concentrations were determined by interpolating from a standard
224 calibration curve generated using known concentrations.

225

226 **Determination of the fraction of antibiotic persister**

227 The determination of antibiotic persister was performed by modifying a protocol described by
228 Drescher *et al*(14). Logarithmic phase cultures of STM WT and STM Δ*pflB* strains were treated
229 with 15X and 25X the minimum inhibitory concentration (MIC) of meropenem (2 and
230 ciprofloxacin. To determine the persister population, aliquots were collected at specified
231 timepoints post-treatment and plated for colony-forming unit (CFU) enumeration. Similarly,
232 24-hour-old biofilm cultures were exposed to the same antibiotic concentrations, and persister
233 cells were quantified via plating. The resulting CFU counts were normalized against the pre-
234 inoculum values to calculate fold viability relative to the 0-hour timepoint. Data were expressed
235 as $\log_{10}$(fold decrease in CFU relative to 0 h).

236

237 **Statistical Analysis**

238 Each experiment was independently repeated between 1 and 12 times, as specified in the figure
239 legends. Statistical analyses were conducted using an unpaired Student's t-test, or two-way
240 ANOVA, as indicated in the respective legends. Data from mouse experiments were analysed
241 using the Mann–Whitney U test. A p-value of less than 0.05 was considered statistically
242 significant. Results are presented as Mean ± SD or Mean ± SEM, as noted in the figure legends.
243 All data analysis and graphical representations were performed using GraphPad Prism version
244 8.4.2.

245

246 ## Results

247 ***pflB* was transcriptionally upregulated in ciprofloxacin resistant mutants, indicating a**
248 **possible involvement of intracellular formate in regulating *Salmonella* AMR**

249 In our earlier work, we demonstrated that *pflB* plays a central role in maintaining ipH in
250 *Salmonella*, which in turn governs the adhesion–invasion switch during its pathogenic lifestyle
251 (10). Other studies have also highlighted the importance of ipH in shaping bacterial
252 antimicrobial responses (15, 16). These observations prompted us to investigate whether
253 intracellular formate levels might also contribute to the regulation of AMR in *Salmonella*.

254 To investigate formate-associated responses, we analysed *pflB* expression in ciprofloxacin-
255 resistant mutants (Cip-R C1, C2, C3) generated by passaging STM for 160 generations under
256 sublethal ciprofloxacin. All Cip-R strains showed increased *pflB* transcription relative to WT
257 **(Figure 1A)**. In Cip-R C1, sublethal ciprofloxacin further improved *pflB* expression **(Figure**
258 **1B)**, which coincided with elevated intracellular formate levels under drug exposure **(Figure**
259 **1C)**.

260 In contrast, meropenem-resistant strains (Mer-R C1, C2, C3), obtained via sublethal
261 meropenem passaging, displayed reduced *pflB* transcription **(Figure 1D)**. However, Mer-R C1
262 and Mer-R C3 upregulated *pflB* upon sublethal meropenem exposure **(Figure 1E)**.
263 Consistently, Mer-R C1 had a higher intracellular concentration formate than the WT strain
264 **(Figure 1F)**. Together, these results indicate that elevated intracellular formate is a recurring
265 feature of strains evolved under ciprofloxacin or meropenem pressure.

266 Since *pflB* encodes pyruvate-formate lyase, the major source of intracellular formate in
267 *Salmonella*, we used cloned *pflB* in the plasmid pQE60 and overexpressed it using Isopropyl
268 β-D-1-thiogalactopyranoside (IPTG) to assess the functional impact of enhanced *pflB* (17). In
269 STM WT, *pflB* overexpression reduced the Propidium Iodide (PI)–positive population—

270 signifying lower cell death—after meropenem treatment, with no effect observed under
271 ciprofloxacin exposure **(Figure 1G)**. *pflB* overexpression also decreased intracellular pH in
272 both untreated and meropenem-treated cells **(Figure 1H)**, consistent with our earlier
273 observation that *pflB* deletion disturbs pH homeostasis.

274 Aligned with these observations, meropenem and ciprofloxacin exposure continued to increase
275 intracellular formate in our laboratory WT strain **(Figure 1I)**. To probe the role of ipH in
276 antibiotic responses, we monitored ipH changes in STM WT and STM Δ*pflB* following
277 sublethal meropenem or ciprofloxacin treatment using the ratiometric dye BCECF-AM. STM
278 WT exhibited a reduced 488/405 ratio under antibiotic stress, indicating cytoplasmic
279 acidification. STM Δ*pflB*, which shows a higher basal ratio, did not acidify upon antibiotic
280 exposure, suggesting resistance to pH drops. Formate supplementation partially rescued the
281 Δ*pflB* phenotype by decreasing the 488/405 ratio under antibiotic stress. Although formate
282 alone had little effect on WT ipH, antibiotic-treated WT displayed an increased 488/405 ratio
283 with formate **(Figure 1J)**. Since PflB converts pyruvate into formate, we found that *pflB*
284 deletion resulted in elevated intracellular pyruvate levels under untreated conditions. These
285 higher pyruvate levels in STM Δ*pflB* persisted during meropenem and ciprofloxacin exposure.
286 In contrast, STM WT strain showed an overall increase in pyruvate upon antibiotic treatment,
287 suggesting that the cell may upregulate *pflB* to channel pyruvate toward formate production as
288 a strategy to counter antibiotic stress by lowering intracellular pH **(Figure S1A)**.

289 Together, these findings indicate that formate is a key metabolite whose intracellular levels
290 commonly rise during antibiotic exposure, and whose depletion disrupts pH homeostasis under
291 antibiotic stress.

292

293 **Deletion of *pflB* enhances susceptibility of STM to meropenem and ciprofloxacin, whereas**
294 **supplementation of extracellular formate also heightens susceptibility of STM to these**
295 **antibiotics**

296 To investigate the impact of deleting *pflB*, which was consistently upregulated during antibiotic
297 exposure, we examined how this gene deletion affected the antibiotic susceptibility of STM.
298 To assess the sensitivity of the STM Δ*pflB* strain to meropenem and ciprofloxacin, both the
299 wild-type and mutant strains were treated with a range of antibiotic concentrations. The STM
300 Δ*pflB* mutant showed significantly increased sensitivity to meropenem, particularly at
301 concentrations of 1 mg/L and 0.5 mg/L **(Figure 2A)**. While the partial restoration of bacterial
302 growth upon sodium formate supplementation was not statistically significant, it suggests that
303 intracellular formate deficiency may contribute to the heightened sensitivity to meropenem.
304 Interestingly, when formate was added to wild-type cells—despite their intact intracellular
305 formate levels—a significant reduction in survivability was observed under antibiotic stress at
306 the same concentrations. Comparable results were obtained with ciprofloxacin, where
307 statistically significant effects were noted at 0.03125, 0.015625, 0.0078, and 0.0039 mg/L
308 **(Figure 2B)**. These findings were further supported by resazurin assay data **(Figure 2C, D)**.
309 The enhanced susceptibility of STM Δ*pflB* and its recovery in the presence of sodium formate
310 was also true for ceftazidime, a third generation cephalosporin (18) **(Figure S1B)**.
311 To investigate how deletion of *pflB* affects STM's antibiotic susceptibility, we treated
312 logarithmic-phase cultures overnight with sub-lethal doses of meropenem (0.5 mg/L) and
313 ciprofloxacin (0.015625 mg/L)and analyzed PI uptake via flow cytometry. STM Δ*pflB* showed
314 a higher PI-positive population than WT, which was significantly reduced with sodium formate
315 supplementation. In contrast, formate supplementation increased PI-positive cells in WT upon
316 antibiotic exposure **(Figure 3A, B)**.

317 We next assessed whether *pflB* deletion and formate supplementation affected susceptibility to
318 additional antibiotics. STM Δ*pflB* displayed increased sensitivity to sub-lethal doses of the
319 fluoroquinolone levofloxacin (1 μg/ml), the carbapenem doripenem (1 μg/ml), and the β-
320 lactam ampicillin (64 μg/ml), with partial restoration of resistance following formate
321 supplementation (19-21). Formate addition to STM WT also heightened susceptibility to these
322 antibiotics **(Figure S2A–C)**. These observations suggest that the increased antimicrobial
323 sensitivity caused by *pflB* deletion or by external formate supplementation may extend beyond
324 meropenem and ciprofloxacin. Nevertheless, to maintain focus and clarity, we concentrated on
325 meropenem and ciprofloxacin in the subsequent analyses.
326 Given that bactericidal antibiotics induce reactive oxygen species (ROS) irrespective of their
327 mechanisms, we assessed intracellular ROS using DCF_2DA staining(22-24). Consistent with
328 PI staining results, STM Δ*pflB* exhibited elevated DCF_2DA-positive populations under
329 antibiotic stress, which was mitigated by formate. Similarly, formate supplementation
330 increased ROS levels in WT cells exposed to antibiotics **(Figure 3C, S3 A)**. These findings
331 suggest that loss of *pflB*, and thus intracellular formate, increases STM's susceptibility to
332 meropenem and ciprofloxacin, while exogenous formate to wild-type cells also enhances
333 antibiotic sensitivity.
334
335 **Deletion of *pflB* was associated with a transcriptional downregulation of antibiotic efflux**
336 **pumps, which was also common for formate supplemented in wild-type cells**
337 Our previous work demonstrated increased membrane depolarization in STM Δ*pflB* compared
338 to WT cells (10). Previous studies have shown that outer membrane of Gram-negative
339 pathogens forms a robust permeability barrier which can prevent antibiotics to reach their target
340 (25). Given that antimicrobial agents like antimicrobial peptides can exert bactericidal effects
341 via membrane depolarization we hypothesized that the enhanced antibiotic susceptibility of

342 STM Δ*pflB* may be attributable, at least in part, to its depolarized membrane state(26-30).
343 Notably, membrane depolarization was further exacerbated upon exposure to sub-lethal
344 concentrations of meropenem and ciprofloxacin, while sodium formate partially alleviated this
345 effect in STM Δ*pflB*. In contrast, formate supplementation had no impact on membrane
346 potential in WT cells under unstressed conditions, although increased depolarization was
347 observed upon antibiotic exposure **(Figure 3D, S3 B)**.
348 Efflux-mediated resistance represents a major mechanism of antibiotic failure in Gram-
349 negative bacteria. *Salmonella* harbors multiple efflux systems, among which the TolC-
350 dependent resistance-nodulation-division (RND) family plays a central role in expelling a
351 broad range of clinically relevant antibiotics(31-34). As proton motive force (PMF) and pH
352 homeostasis are critical for the functioning of these pumps, and membrane depolarization can
353 disrupt PMF, we hypothesized that the reduced antibiotic efflux in STM Δ*pflB* may stem from
354 impaired PMF(11). To test this, we employed a nile red efflux assay. STM Δ*pflB* retained
355 significantly higher levels of nile red fluorescence, indicating decreased efflux activity.
356 Formate supplementation reduced nile red retention, suggesting partial restoration of efflux
357 capacity. Similarly, formate-treated STM WT cells exhibited increased nile red fluorescence
358 upon antibiotic exposure, consistent with reduced efflux function **(Figure 3E)**.
359 To determine whether reduced efflux activity was due solely to membrane depolarization or
360 also involved transcriptional regulation, we measured mRNA levels of *acrB* and *tolC*, two key
361 components of the RND efflux system in *Salmonella*(35). Deletion of *pflB* resulted in
362 transcriptional downregulation of both genes, with partial recovery upon formate
363 supplementation. Interestingly, formate supplementation in STM WT also led to reduced *acrB*
364 and *tolC* expression **(Figure 3F, G)**. These findings suggest that while membrane
365 depolarization may directly impair efflux pump activity, additional transcriptional regulatory
366 mechanisms may also contribute to reduced efflux and heightened antibiotic susceptibility.

367 Outer membrane proteins (Omps) influence antibiotic susceptibility in *Salmonella*, with
368 reduced OmpF expression typically linked to resistance (36-38). Notably, *ompF* was
369 downregulated in STM Δ*pflB* **(Figure 3H)**, even though this strain showed increased antibiotic
370 sensitivity. This indicates that the heightened susceptibility of STM Δ*pflB* occurs independently
371 of Omps, as decreased OmpF would normally correlate with resistance rather than greater
372 sensitivity.
373

374 **Formate supplementation in drinking water and intrabacterial formate deficiency both**
375 **enhanced bacterial clearance by antibiotics *in-vivo***

376 We tested whether our *in-vitro* results also applied in living animals by giving C57BL/6 mice
377 an oral dose of 10^6 CFU of STM WT or STM Δ*pflB*. The mice also received 125 mM sodium
378 formate in their drinking water **(Figure 4A)**. Earlier work suggests that mice need about 40
379 mmol of formate per day. Since C57BL/6 mice usually drink around 30 ml of water daily, they
380 would need about a 1 M solution to reach that amount. However, previous studies showed that
381 500 mM sodium formate can cause weight loss, so we selected a safer dose of 125 mM,
382 representing about 10% of the estimated daily requirement (39). In our pilot tests, this amount
383 was enough to significantly raise serum formate levels by 5 days post-infection **(Figure S4A)**.
384 Our findings showed that adding formate to the drinking water together with meropenem
385 treatment lowered bacterial loads more than meropenem alone in the intestine, liver, and spleen
386 of C57BL/6 mice. As expected, the STM Δ*pflB* mutant showed reduced organ colonization
387 (10); but formate supplementation did not restore its numbers. Meropenem further reduced the
388 bacterial load, and—unlike our *in-vitro* results—formate did not rescue the decreased bacterial
389 counts. Interestingly, combining formate with meropenem did not lower organ colonization in
390 STM Δ*pflB* the way it did in STM WT, suggesting that STM Δ*pflB* may use extracellular
391 formate to survive antibiotic stress (**Figure 4B**). The same trends were seen with ciprofloxacin

392 (**Figure 4C**) and ceftazidime (**Figure 4D**) in mice infected with STM WT or STM Δ*pflB* under
393 formate-supplemented conditions.
394
395 **Deletion of *rpoE* from STM Δ*pflB* reversed the enhanced antibiotic susceptibility,**
396 **associated with a recovery in the transcript levels of *acrB* and *tolC***
397 In *E. coli*, RpoE (σ^E) functions as an extra cytoplasmic stress sigma factor essential for viability
398 and for coordinating the cellular response to membrane stress (40). The membrane protein
399 RseA, together with the periplasmic factor RseB, binds and sequesters σ^E under non-stress
400 conditions, preventing its interaction with RNA polymerase (41, 42). When envelope stress
401 occurs, RseA—which is intrinsically unstable—is rapidly degraded, releasing σ^E to activate its
402 target genes. These genes support the synthesis, transport, and assembly of
403 lipopolysaccharides, phospholipids, and outer membrane proteins (OMPs), as well as proteases
404 and chaperones required to preserve or restore outer membrane integrity (42-45). Recent
405 studies further demonstrate that σ^E indirectly increases the transcription of the sRNAs *csrB* and
406 *csrC* through σ^{70}-dependent promoters (46, 47)

407 In our previous work, we demonstrated that deletion of *pflB* disrupts intracellular pH
408 homeostasis, leading to membrane depolarization. This perturbation activated the
409 extracytoplasmic sigma factor RpoE, which in turn upregulated transcription of the small RNA
410 *csrB*. The *csrB* RNA can antagonize the activity of the global regulator CsrA by direct binding,
411 thereby impairing processes such as flagellar biosynthesis (10). Notably, CsrA has been shown
412 to stabilize the *acrAB* transcript by interacting with its 5′ untranslated region (48). Given the
413 increased membrane depolarization observed in STM Δ*pflB* upon antibiotic exposure, we
414 hypothesized that RpoE may regulate *acrB* expression indirectly through modulation of the
415 CsrA–*csrB* regulatory circuit.

416 To test this, we exposed the STM Δ*pflB*Δ*rpoE* strain to sublethal concentrations of meropenem
417 and ciprofloxacin. Compared to STM Δ*pflB*, the double knockout exhibited a significantly
418 reduced proportion of PI-positive cells **(Figure 5A, B)**. Interestingly, deletion of *rpoE* in the
419 STM Δ*pflB* background did not restore membrane potential under basal conditions. However,
420 upon antibiotic challenge, we observed a significant reduction in $DiBAC_4$-positive cells,
421 indicative of partial recovery in membrane polarization **(Figure 5C, S5A)**. However STM
422 Δ*pflB*Δ*rpoE* had a decreased ROS positive cells compared to STM Δ*pflB*, as assessed using
423 DCF_2DA staining **(Figure 5D, S5B)**. This was consistent with a decrease in the heightened ipH
424 of STM Δ*pflB* following treatment with ciprofloxacin and meropenem when *rpoE* was
425 simultaneously deleted **(Figure S4B)**.
426 The improved viability of STM Δ*pflB*Δ*rpoE* relative to STM Δ*pflB* under antibiotic stress was
427 further supported by atomic force microscopy, which revealed increased cellular length and
428 height following exposure to both meropenem and ciprofloxacin **(Figure S6A-C)**.
429 These phenotypic changes correlated with the restoration of *acrB* and *tolC* transcript levels in
430 STM Δ*pflB*Δ*rpoE*, suggesting enhanced efflux activity **(Figure 5E, F)**. This was further
431 confirmed by increased nile red efflux, indicative of improved pump function **(Figure 5G)**.
432 Given the role of EmrB in fluoroquinolone resistance, we also examined its expression **(Figure
433 5H)** (49). As previous studies have not identified a direct regulatory relationship between CsrA
434 and *emrB*, we measured *emrB* transcript levels and observed no significant change in STM
435 Δ*pflB*Δ*rpoE* relative to STM Δ*pflB*. These findings suggest that the observed phenotypic rescue
436 is primarily mediated through the CsrA–*csrB* axis. Deletion of *rpoE* in STM Δ*pflB* led to
437 further downregulation of *ompF*, indicating that while *ompF* suppression does not explain the
438 increased antibiotic sensitivity of STM Δ*pflB*, its further downregulation upon *rpoE* deletion
439 may contribute to the restored resistance observed in STM Δ*pflB*Δ*rpoE* **(Figure 5I)**.

440 A comparable reduction in CFU for all the strains following 10 mM glutathione antioxidant
441 under sublethal meropenem and ciprofloxacin exposure indicates that the observed differences
442 in bacterial killing are attributable to the distinct levels of ROS generated by each antibiotic
443 **(Figure S7A, B)**(50).
444

445 **Deletion of *sirA* abolishes the antibiotic susceptibility of STM Δ*pflB*, along with reduction**
446 **in ROS levels and membrane depolarization**

447 To further confirm that small RNA *csrB* regulates antibiotic susceptibility, we examined an
448 additional upstream regulator of *csrB*. The BarA/SirA two-component system, which is also
449 known to activate the expression of *csrB* and *csrC* small RNAs, has previously been shown to
450 enhance the expression of HilD, a key regulator of genes within the *Salmonella* Pathogenicity
451 Island-1 (51-53). We deleted *sirA* in the STM Δ*pflB* background and used flow cytometry to
452 quantify propidium iodide-positive cells, revealing a marked reduction in dead cells in the STM
453 Δ*pflB*Δ*sirA* strain compared to STM Δ*pflB* **(Figure 6A, B)**. Interestingly, this decrease in cell
454 death did not correspond with a reduction in membrane depolarization, indicating that the
455 reduced antibiotic sensitivity in STM Δ*pflB*Δ*sirA* was independent of changes in membrane
456 potential **(Figure 6C, S8A)**. A drop in DCF_2DA-positive cells further supported the observation
457 of diminished antibiotic susceptibility following *sirA* deletion in STM Δ*pflB*. Notably, STM
458 Δ*sirA* alone showed an increase in DCF_2DA-positive cells after exposure to meropenem and
459 ciprofloxacin **(Figure 6D, S8B)**. This prompted an investigation into efflux pump expression.
460 We observed that *sirA* deletion in STM Δ*pflB* led to elevated expression of *acrB*, *tolC*, *emrB*,
461 and *ompF* **(Figure 6 E-H)**. A nile red assay confirmed restored efflux pump activity in STM
462 Δ*pflB*Δ*sirA* **(Figure 6I)**. Interestingly, deletion of *sirA* alone resulted in decreased *acrB*
463 transcript levels, which may explain the increased DCF_2DA-positive population upon
464 treatment with meropenem and ciprofloxacin in STM Δ*sirA* **(Figure 6 E)**. However, no overall

465 change in efflux activity was detected in STM Δ*sirA*, possibly due to compensatory roles by
466 other efflux pumps **(Figure 6I)**. These findings suggest that targeting upstream regulators of
467 *csrB* can effectively reverse the antibiotic susceptibility observed in STM Δ*pflB*.
468

469 **Deletion of *sirA* ameliorates the heightened susceptibility of STM WT to antibiotics upon**
470 **exogenous F supplementation.**

471 The BarA/SirA two-component regulatory system functions by directly promoting increased
472 expression of the small regulatory RNA *csrB* (54). Given that CsrA is a key regulator of *acrAB*
473 transcript expression, we aimed to determine whether formate-induced signalling through the
474 BarA/SirA system contributes to the enhanced antibiotic sensitivity observed in STM WT (48).
475 To explore this, we assessed the antibiotic susceptibility of the STM Δ*sirA* in the presence of
476 formate.

477 Formate exposure in STM WT resulted in reduced transcript levels of other efflux-related
478 genes, such as *tolC* and *emrB*. The absence of *sirA* mitigated the suppression of efflux pump
479 gene expression induced by formate in STM WT. Transcript analysis revealed that formate
480 supplementation improved *acrB* expression in STM Δ*sirA*, contrasting with the
481 downregulation of *acrB* seen in formate-treated STM WT **(Figure S9 A-C)**. This reflected in
482 efflux pump activity as well **(Figure S9 D)**.

483 Consistent with previous data, STM WT treated with formate showed a higher percentage of
484 PI-positive cells following exposure to meropenem and ciprofloxacin. Although STM Δ*sirA*
485 showed a PI-positive population comparable to STM WT when exposed to these antibiotics,
486 adding formate did not further increase PI-positive cells in the mutant under ciprofloxacin
487 treatment. In the case of meropenem treatment, a decrease in extent of PI-positive population
488 was observed **(Figure S9 E**). Likewise, formate treatment did not elevate the ROS-positive

489 population in STM Δ*sirA*, unlike the increase observed in STM WT **(Figure S9 F)**. A similar
490 trend was seen in the number of depolarized cells under antibiotic stress **(Figure S9 G)**.

491 In summary, these results suggest that extracellular formate enhances STM WT susceptibility
492 to meropenem and ciprofloxacin primarily through the BarA/SirA signalling system.

493

494

495 **Deletion of *pflB* impaired the long-term survival of STM under high antibiotic**
496 **concentrations, a similar effect observed when formate was supplemented to the wild type**
497 Bacterial persistence in the presence of antibiotics, distinct from antibiotic resistance, remains
498 a persistent challenge in effectively eliminating pathogens in clinical settings(55). Since our
499 data demonstrated that *pflB* deletion increased the antibiotic susceptibility of STM, we aimed
500 to investigate its impact on long-term bacterial survival under high antibiotic stress. Log-phase
501 bacterial cultures, with or without formate supplementation, were exposed to 15× and 25× MIC
502 concentrations of meropenem and ciprofloxacin. Exposure to 15× MIC of meropenem led to a
503 rapid decline in bacterial countsin planktonic culture, with STM Δ*pflB* exhibiting the fastest
504 reduction, reaching statistical significance at 24 hours post-treatment **(Figure 7A)**. Formate
505 supplementation restored survival levels of STM Δ*pflB* to those of the wild type, while
506 supplementation in STM WT also caused a significant reduction in CFUs. This effect was
507 specific to planktonic cultures treated with meropenem and was not observed in biofilm forms
508 or in ciprofloxacin-treated planktonic and biofilm cultures **(Figure 7B, C, D)**.

509

510 Discussion

511 *Salmonella* has emerged as a major food-borne pathogen with widespread drug resistance, and
512 the increasing prevalence of MDR strains poses a serious clinical challenge (56-58). The
513 growing inefficacy of existing treatments complicates disease management and highlights the

514 urgent need for novel antimicrobial strategies or repurposing of existing drugs (59, 60).
515 Traditionally, research on AMR has focused on canonical molecular mechanisms by which
516 bacteria evade antibiotics, including target modification, enzymatic drug degradation, and
517 altered membrane permeability (61-66).
518 More recently, bacterial metabolism has gained attention as a determinant of AMR. For
519 example, ceftriaxone-resistant *Salmonella* Derby was shown to exhibit altered metabolic
520 activity, particularly in glutathione biosynthesis, with reduced levels of oxidized glutathione
521 and citrulline. Supplementation of these metabolites restored ceftriaxone susceptibility in MDR
522 isolates (67). Parallel studies have highlighted the influence of ipH on antibiotic resistance in
523 *Salmonella* and other bacteria (11, 15, 16, 68), underscoring the importance of metabolic
524 pathways involved in pH regulation.
525 The enzyme PflB, which converts pyruvate into formate and acetyl-CoA, plays a central role
526 in maintaining ipH (10). Consistent with this function, we observed that STM lacking *pflB*
527 exhibited increased susceptibility to ciprofloxacin and meropenem, a phenotype that could be
528 partially rescued by external formate supplementation. While pH is known to modulate the
529 PMF and thereby influence efflux activity, our data indicate an additional transcriptional effect,
530 as ipH disruption resulted in downregulation of efflux pump genes *acrB* and *tolC* (11).
531 In previous work, we showed that membrane stress induced by ipH imbalance activated the
532 RpoE sigma factor, elevating expression of the small RNA *csrB* and repressing flagellar gene
533 expression in STM Δ*pflB* (10). In this study, we extend those findings by showing that *rpoE*
534 deletion not only restored motility but also reversed the heightened antibiotic sensitivity of
535 STM Δ*pflB*. Similarly, deletion of *sirA*, an upstream regulator of *csrB*, had a comparable effect.
536 These results suggest that *pflB* regulates both invasion and antibiotic resistance through a
537 shared RpoE–*csrB* signaling pathway. Importantly, we also found that extracellular formate
538 impacts AMR through the BarA/SirA two-component system—traditionally known for its role

539 in regulating invasion—thereby expanding the functional scope of this signaling axis to include
540 efflux-mediated antibiotic resistance (69) **(Graphical abstract)**.
541 The role of metabolism in antibiotic tolerance and persistence has also been documented in
542 other bacteria. In *E. coli*, adenosine was shown to suppress the stringent response, enhance
543 PMF, increase respiration, and sensitize persister cells to antibiotics—a process described as
544 "persister awakening" (70). To test whether formate metabolism influences persistence, we
545 assessed long-term survival of STM Δ*pflB* under high-dose antibiotic treatment. In planktonic
546 cultures, STM Δ*pflB* exhibited accelerated killing compared to the wild type, a phenotype that
547 was reversed by formate supplementation. Interestingly, addition of formate to wild-type STM
548 further enhanced antibiotic killing.
549 Together, our findings support the idea that antibiotic effectiveness is intimately linked to
550 bacterial metabolic state. Specifically, intracellular formate, regulated by PflB, modulates ipH
551 homeostasis, efflux pump expression, and antibiotic tolerance in STM. These results identify
552 formate metabolism as a determinant of both acute resistance and persistence, pointing to
553 metabolic reprogramming as a potential therapeutic strategy to re-sensitize MDR *Salmonella*
554 to existing antibiotics.
555

556 **Acknowledgements**

557 We thank the Departmental Real-Time PCR, Divisional Mass Spectrometry, Divisional Flow
558 Cytometry Facility, Divisional Atomic Force Microscopy, and the Central Animal Facility at
559 IISc for supporting experimental work. Dr. Sunitha assisted in formate quantification via GC-
560 MS. Flow cytometry data acquisition was supported by Mr. Munish and Mrs. Navya. Atomic
561 Force Microscopy was supported by Mrs. Monisha. Dr. Raju Rajmani is acknowledged for help
562 in mice serum isolation.
563

Author Contributions

DM and DC conceived the study and designed the experiments. DM conducted all experiments, data acquisition, analysis, figure preparation, and wrote the original draft. SVW, PG, and AB helped DM with experiments. DM and DC contributed to manuscript editing. DC supervised the project and secured funding. All authors reviewed and approved the final manuscript.

Declaration of Interest

The authors declare no conflicts of interest.

Funding Information

We gratefully acknowledge financial support from the Department of Biotechnology (DBT) and the Department of Science and Technology (DST), Ministry of Science and Technology. DC thanks DAE for the SRC Outstanding Investigator Award, ASTRA Chair Professorship, and TATA Innovation Fellowship. Additional support came from the DBT-IISc Partnership Program. Infrastructure support from ICMR (Molecular Medicine Center), DST (FIST), and UGC-CAS is also acknowledged. DM is supported by IISc fellowship. PG is supported by DBT-JRF fellowship. AB acknowledges UGC fellowship. The funders had no involvement in study design, data collection, analysis, or publication decisions.

Data Availability

Data supporting this study are available from the authors upon request.

589 **Figures and figure legends**

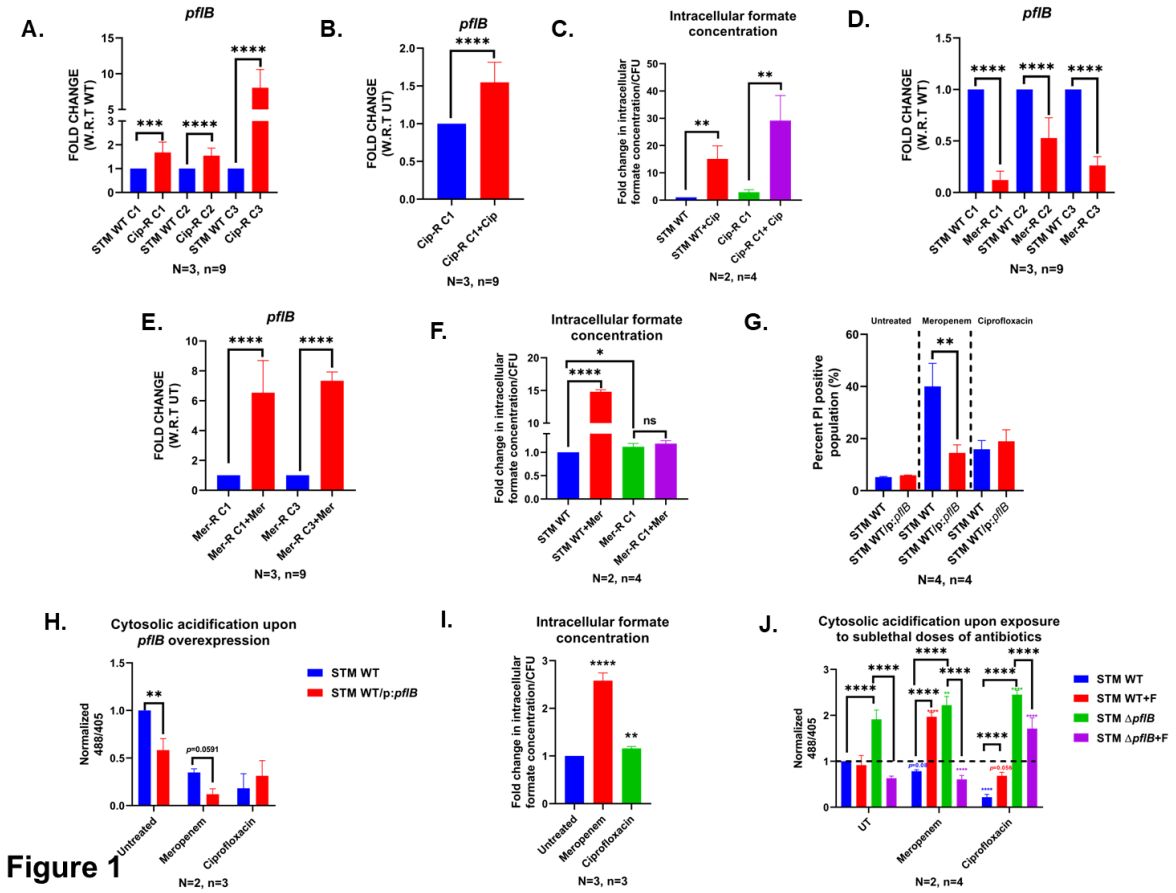

590 **Figure 1**

591 **Figure 1: Higher *pflB* transcription in the presence of antibiotics was frequently observed**
592 **as a characteristic of ciprofloxacin and meropenem mutants, and loss of *pflB* was linked**
593 **to impaired acid homeostasis when exposed to sublethal concentrations of meropenem**
594 **and ciprofloxacin.**

595 (A) Transcriptional upregulation of *pflB* in Cip-R 1, 2, 3 ciprofloxacin resistant STM strains.
596 Data representative of N=3, n=9 and is presented as mean+/- SD.

597 (B) Transcriptional upregulation of *pflB* in Cip-R C1 upon exposure to sub-lethal doses of
598 ciprofloxacin. Data representative of N=3, n=9 and is presented as mean+/- SD.

599 (C) Quantification of intracellular formate levels in STM WT and Cip-R C1 strains upon
600 exposure to sub-lethal dose of ciprofloxacin. Data representative of N=2, n=4 and is presented
601 as mean+/- SD.

602 (D) Transcriptional levels of *pflB* in Mer-R C1, 2, 3 meropenem resistant STM strains. Data
603 representative of N=3, n=9 and is presented as mean+/- SD.
604 (E) Transcriptional upregulation of *pflB* in Mer-R C1, 3 upon exposure to sub-lethal doses of
605 ciprofloxacin. Data representative of N=3, n=9 and is presented as mean+/- SD.
606 (F) Quantification of intracellular formate levels in STM WT and Mer-R C1 strains upon
607 exposure to sub-lethal dose of ciprofloxacin. Data representative of N=2, n=4 and is presented
608 as mean+/- SD.
609 (G) Bar graphs showing PI-positive population in STM WT and STM WT/pQE60:*pflB* upon
610 exposure to meropenem and ciprofloxacin. Data representative of N=2, n=4 and is presented
611 as mean+/- SD.
612 (H) Normalized 488/405 ratio of STM WT and STM WT/pQE60:*pflB* in presence of sub-lethal
613 doses of meropenem and ciprofloxacin. Data representative of N=2, n=4 and is presented as
614 mean+/- SD.
615 (I) Quantification of intracellular formate levels in STM WT upon exposure to sub-lethal dose
616 of ciprofloxacin and meropenem. Data representative of N=3, n=3 and is presented as mean+/-
617 SD.
618 (J) Normalized 488/405 ratio of STM WT and STM Δ*pflB* in presence of sub-lethal doses of
619 meropenem and ciprofloxacin. Data representative of N=2, n=4 and is presented as mean+/-
620 SD.
621 (Unpaired two-tailed Student's t-test for column graphs, Two-way ANOVA for grouped data,
622 Mann-Whitney U-test for animal experiment data (*** $p < 0.0001$, *** $p < 0.001$, ** $p<0.01$,
623 * $p<0.05$))
624

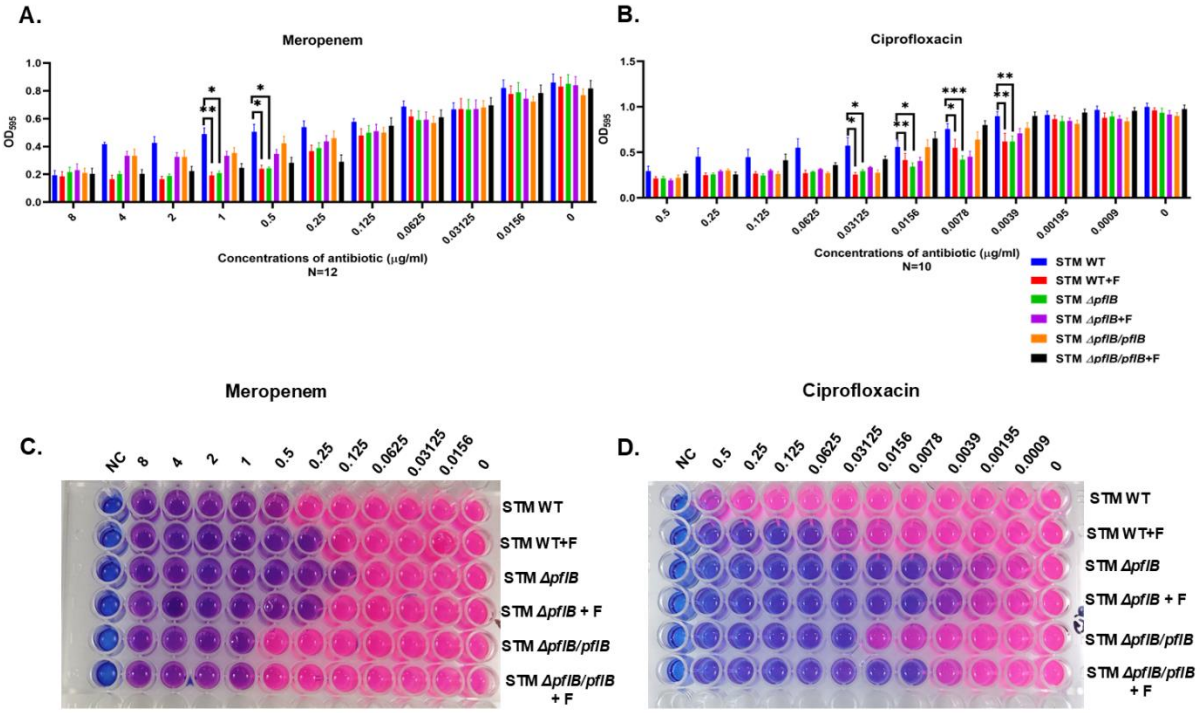

Figure 2

Figure 2: Deletion of *pflB* increases STM's sensitivity to meropenem and ciprofloxacin, while extracellular formate supplementation similarly enhances antibiotic susceptibility.

(A) Meropenem susceptibility of STM WT, STM Δ*pflB*, and STM Δ*pflB*/pQE60: *pflB*, with or without formate treatment, was assessed using the microfold dilution method. Data presented as mean+/- SEM of N=12.

(B) Ciprofloxacin susceptibility of STM WT, STM Δ*pflB*, and STM Δ*pflB*/pQE60: *pflB*, with or without formate treatment, was assessed using the microfold dilution method. Data presented as mean+/- SEM of N=10.

(C) Resazurin assay of STM WT, STM Δ*pflB*, and STM Δ*pflB*/pQE60: *pflB*, with or without formate treatment, in increasing concentrations of meropenem.

636 (D) Resazurin assay of STM WT, STM Δ*pflB*, and STM Δ*pflB*/pQE60: *pflB*, with or without

637 formate treatment, in increasing concentrations of ciprofloxacin.

638 (Unpaired two-tailed Student's t-test for column graphs, Two-way ANOVA for grouped data,

639 Mann-Whitney U-test for animal experiment data (*** $p < 0.0001$, *** $p < 0.001$, ** $p<0.01$,

640 * $p<0.05$))

641

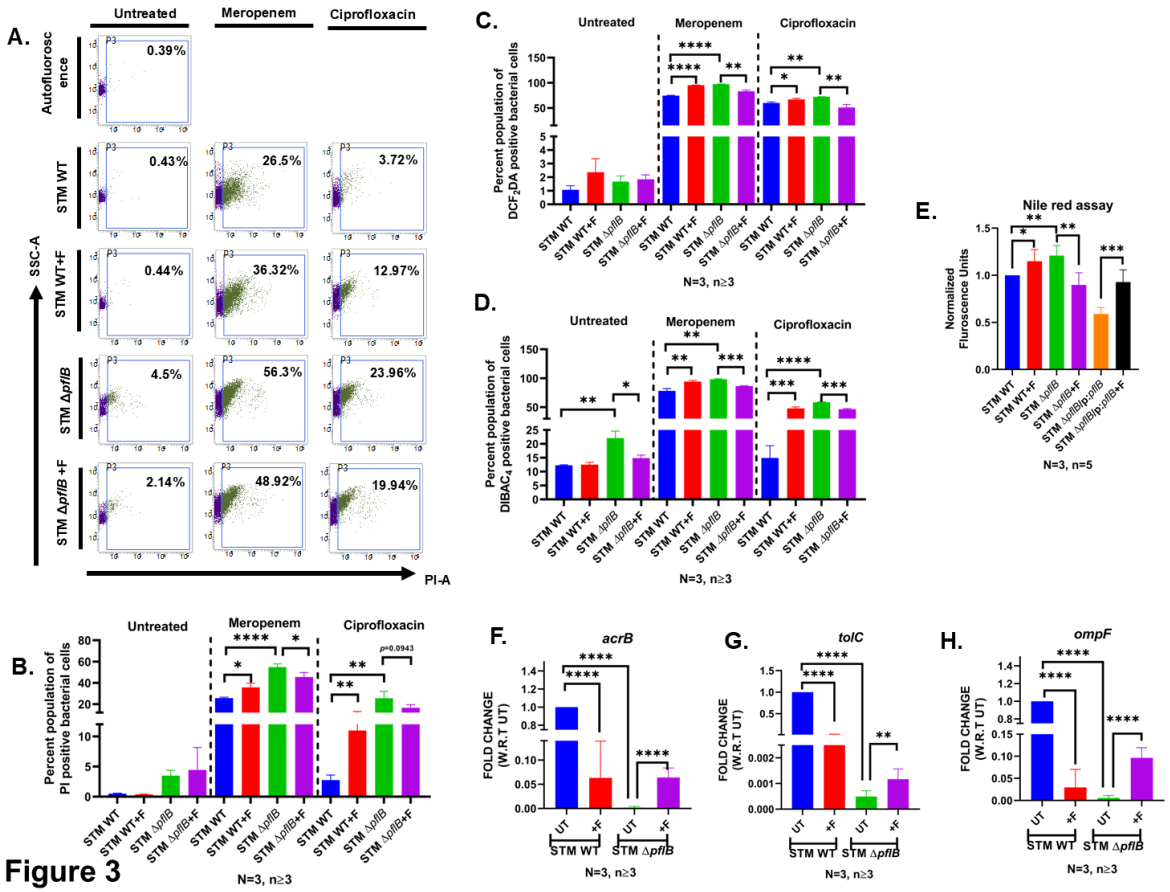

642 Figure 3

643 **Figure 3: Increased antibiotic sensitivity following *pflB* deletion was linked to**

644 **transcriptional downregulation of efflux pumps, a pattern also observed in formate-**

645 **treated wild-type cells.**

646 (A) Dot plots (SSC-A vs PI-A) and bar graph illustrate increased bacterial killing with

647 meropenem and ciprofloxacin following *pflB* deletion and formate supplementation in STM

648 WT. Data representative of N=3, n≥3.

649 (B) Bar graphs depict the PI-positive population after exposure to meropenem and
650 ciprofloxacin following *pflB* deletion and formate supplementation in STM WT. Data represent
651 N=3, n≥3 and are shown as mean ± SD.
652 (C) Bar graphs display the $DiBAC_4$-positive population under meropenem and ciprofloxacin
653 treatment after *pflB* deletion and formate supplementation in STM WT. Data represent N=3,
654 n≥3 and are shown as mean ± SD.
655 (D) Bar graphs present the DCF_2DA-positive population upon exposure to meropenem and
656 ciprofloxacin following *pflB* deletion and formate supplementation in STM WT. Data represent
657 N=3, n≥3 and are shown as mean ± SD.
658 (E) Nile red assay quantifies efflux pump activity in STM WT, STM Δ*pflB, and* STM
659 Δ*pflB*/pQE60:*pflB* . Data representative of N=3, n=5 and is presented as mean+/- SD.
660 (F-H) Transcript levels of *acrB*, *tolC*, and *ompF* measured in STM WT and STM Δ*pflB*, with
661 or without formate treatment. Data representative of N=3, n≥3 and is presented as mean+/- SD.
662 (Unpaired two-tailed Student's t-test for column graphs, Two-way ANOVA for grouped data,
663 Mann-Whitney U-test for animal experiment data (*** $p < 0.0001$, *** $p < 0.001$, ** $p<0.01$,
664 * $p<0.05$))
665

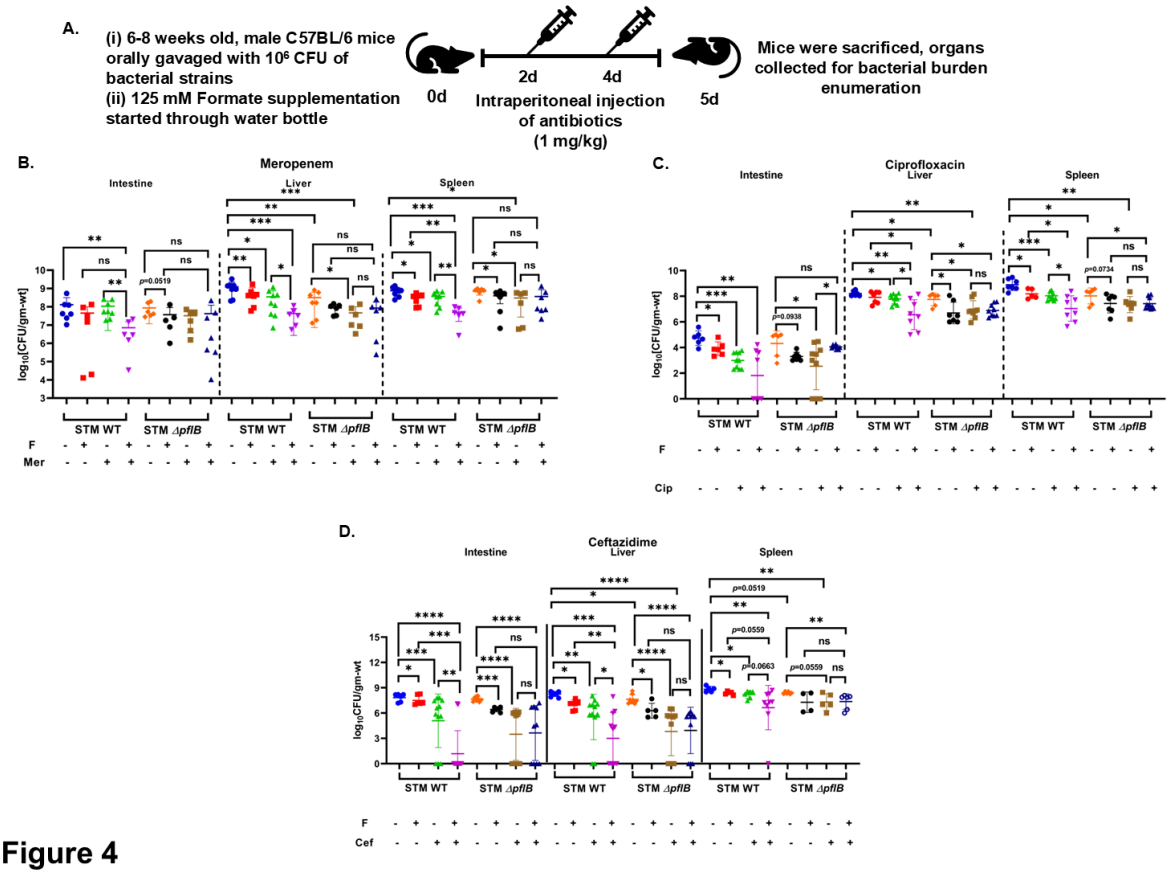

Figure 4

Figure 4: Both formate supplementation via drinking water and internal formate deficiency enhanced antibiotic-mediated bacterial clearance *in vivo*.

(A) Schematic outlining the experimental design.

(B-D) Role of formate supplementation in STM WT and STM Δ*pflB* clearance from the intestine, liver, and spleen following treatment with meropenem, ciprofloxacin, and ceftazidime. Data representative of N≥8 and is presented as mean+/- SD.

(Unpaired two-tailed Student's t-test for column graphs, Two-way ANOVA for grouped data, Mann-Whitney U-test for animal experiment data (*** $p < 0.0001$, *** $p < 0.001$, ** $p<0.01$, * $p<0.05$))

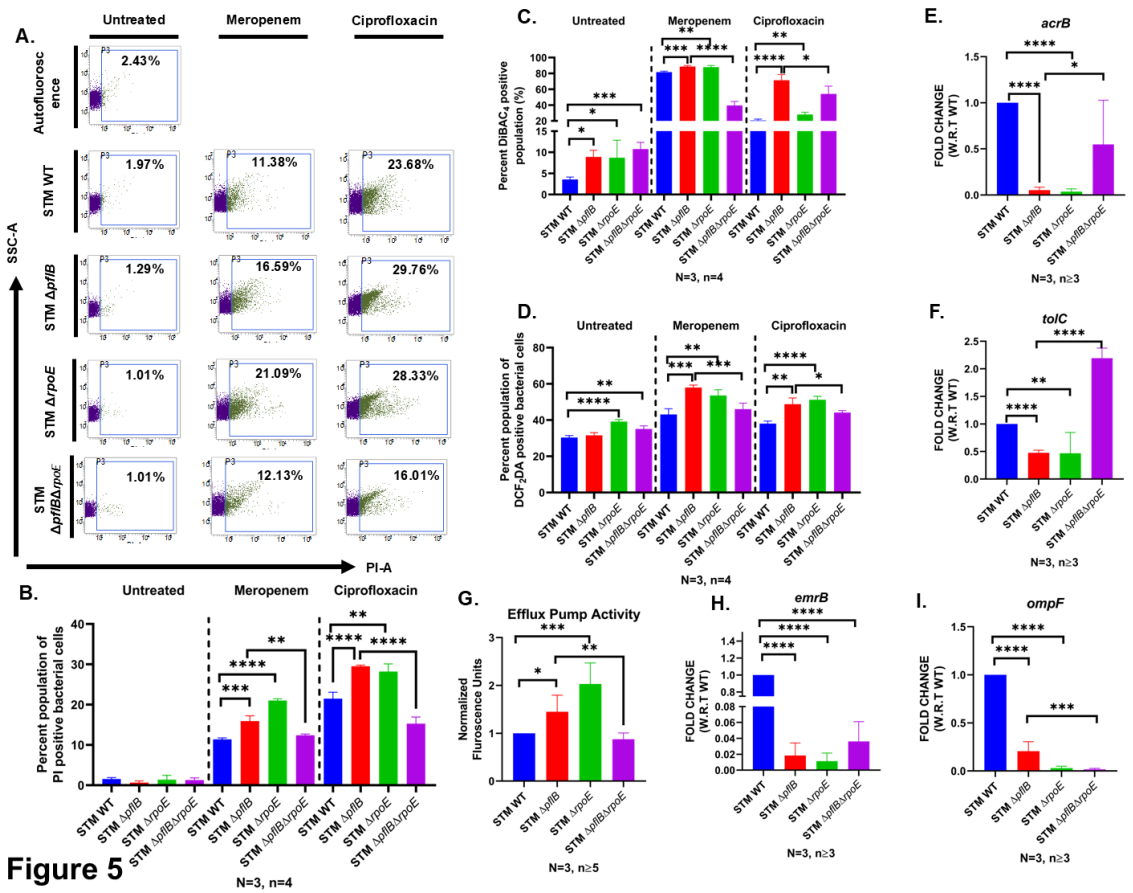

Figure 5

Figure 5: Deletion of *rpoE* in STM Δ*pflB* reversed its increased antibiotic sensitivity, accompanied by restored *acrB* and *tolC* transcript levels.

(A) Dot plots (SSC-A vs PI-A) showing antibiotic-mediated killing in STM Δ*pflB* upon *rpoE* deletion. Data representative of N=3, n=4.

(B) Bar graphs showing PI positive population in STM Δ*pflB* upon *rpoE* deletion and upon exposure to sub-lethal doses of meropenem and ciprofloxacin. Data representative of N=3, n=4 and is presented as mean+/- SD.

(C) Bar graphs display the $DiBAC_4$-positive population under meropenem and ciprofloxacin treatment after *rpoE* deletion in STM Δ*pflB*. Data represent N=3, n=4 and are shown as mean ± SD.

(D) Bar graphs present the DCF_2DA-positive population upon exposure to meropenem and ciprofloxacin following *rpoE* deletion in STM Δ*pflB*. Data represent N=3, n=4 and are shown as mean ± SD.

692 (E-F) Transcript levels of key efflux pump genes *acrB* and *tolC* were compared between STM

693 Δ*pflB*Δ*rpoE* and STM Δ*pflB*. Data representative of N=3, n≥3 and is presented as mean+/- SD.

694 (G) Efflux activity assessed using the Nile red assay. Data representative of N=3, n≥5 and is

695 presented as mean+/- SD.

696 (H-I) Transcriptional expression of *emrB* and *ompF* was also evaluated. Data representative of

697 N=3, n≥3 and is presented as mean+/- SD.

698 (Unpaired two-tailed Student's t-test for column graphs, Two-way ANOVA for grouped data,

699 Mann-Whitney U-test for animal experiment data (*** $p < 0.0001$, *** $p < 0.001$, ** $p<0.01$,

700 * $p<0.05$))

701

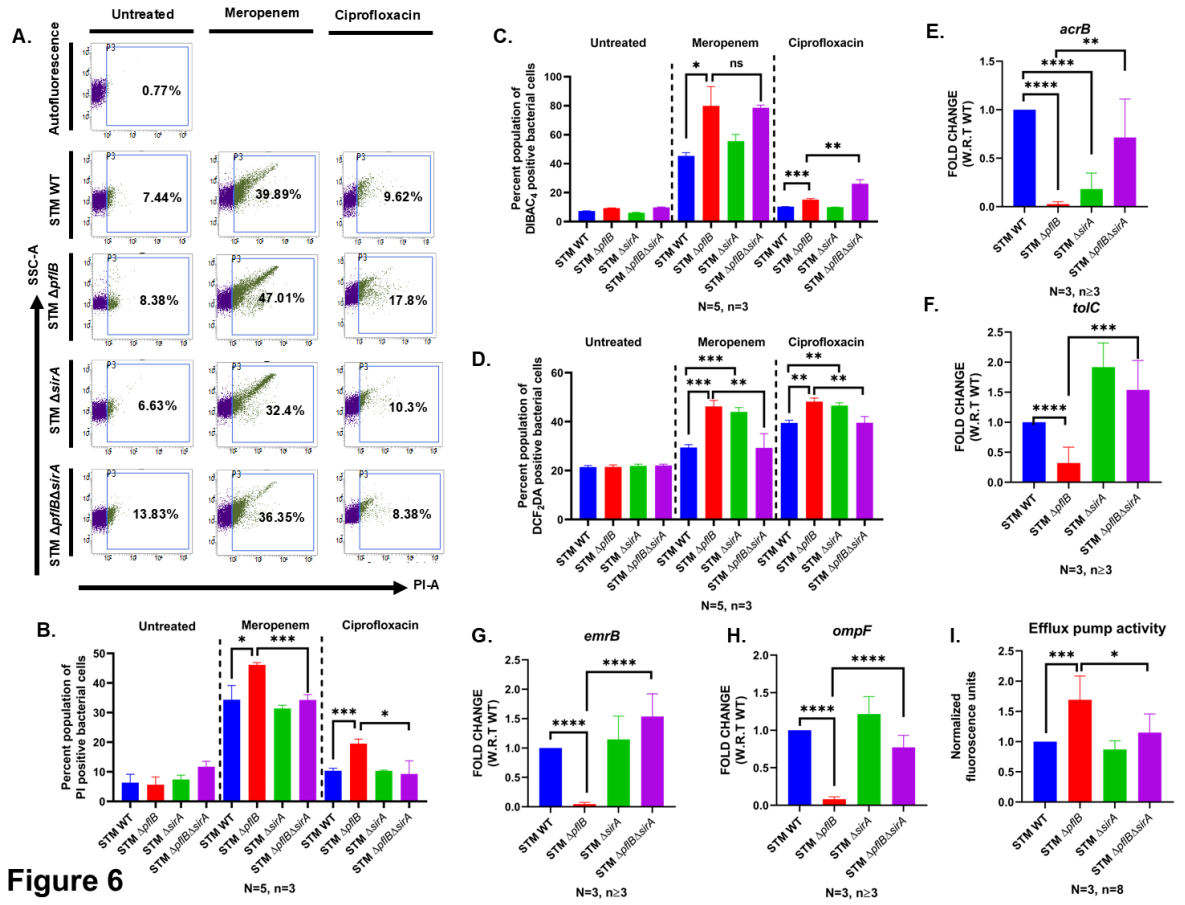

Figure 6

702

703 **Figure 6: Deleting *sirA* in STM Δ*pflB* similarly reversed its heightened antibiotic**

704 **sensitivity and restored *acrB* and *tolC* expression levels.**

705 (A) Dot plots (SSC-A vs PI-A) showing reduced antibiotic-mediated killing in STM Δ*pflB*
706 upon *sirA* deletion. Data representative of N=5, n=3.
707 (B) Bar graphs showing antibiotic-mediated killing in STM Δ*pflB* upon *sirA* deletion. Data
708 representative of N=5, n=3 and is presented as mean+/- SD.
709 (C) Bar graphs showing $DiBAC_4$ population in STM Δ*pflB* upon *sirA* deletion and exposure to
710 antibiotics. Data representative of N=5, n=3 and is presented as mean+/- SD.
711 (D) Bar graphs showing DCF_2DA population in STM Δ*pflB* upon *sirA* deletion and exposure
712 to antibiotics. Data representative of N=5, n=3 and is presented as mean+/- SD.
713 (E-H) Transcript levels of efflux pump genes *acrB, tolC*, *emrB,* and *ompF* were compared
714 between STM Δ*pflB*Δ*sirA* and STM Δ*pflB*. Data representative of N=3, n≥3 and is presented
715 as mean+/- SD.
716 (I) Efflux activity assessed using the Nile red assay. Data representative of N=3, n=8 and is
717 presented as mean+/- SD.
718 (Unpaired two-tailed Student's t-test for column graphs, Two-way ANOVA for grouped data,
719 Mann-Whitney U-test for animal experiment data (*** $p < 0.0001$, *** $p < 0.001$, ** $p<0.01$,
720 * $p<0.05$))
721

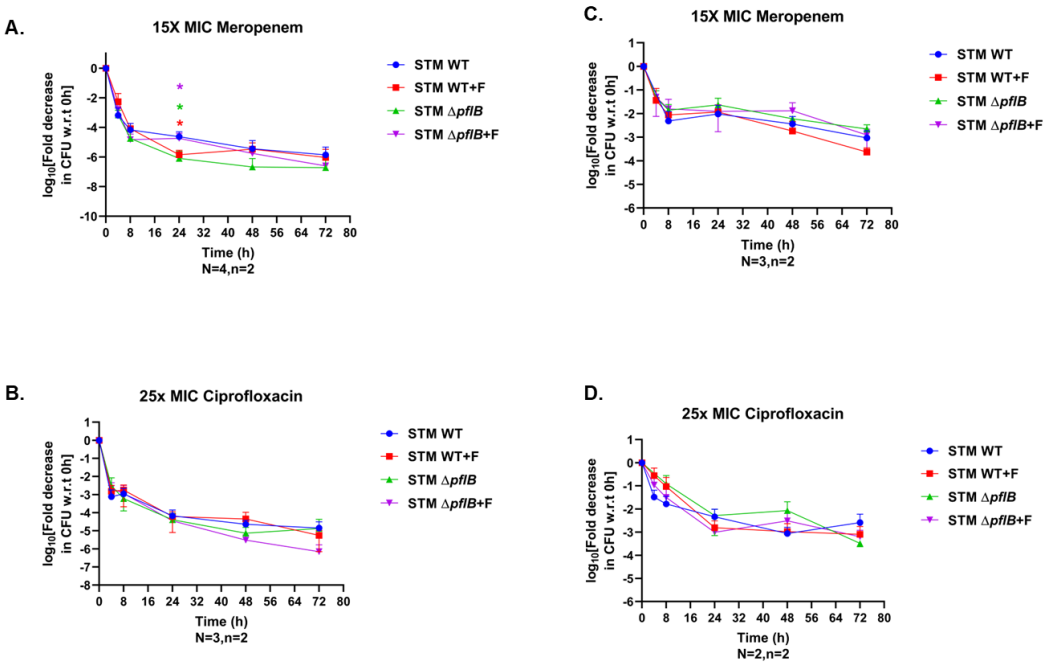

Figure 7

Figure 7: Deletion of *pflB* reduced STM's long-term survival under high antibiotic concentrations, an effect also seen with formate supplementation in the wild type.

(A,B) Line graphs show log_{10} fold reduction in CFU relative to 0h for planktonic cultures of STM WT and STM Δ*pflB*, with or without formate supplementation, upon exposure to 15X MIC of meropenem and 25X MIC of ciprofloxacin. Data is presented as mean+/- SD.

(C, D) Line graphs show log_{10} fold reduction in CFU relative to 0h for biofilm cultures of STM WT and STM Δ*pflB*, with or without formate supplementation, upon exposure to 15X MIC of meropenem and 25X MIC of ciprofloxacin. Data is presented as mean+/- SD.

(Unpaired two-tailed Student's t-test for column graphs, Two-way ANOVA for grouped data, Mann-Whitney U-test for animal experiment data (*** $p < 0.0001$, *** $p < 0.001$, ** $p<0.01$, * $p<0.05$))

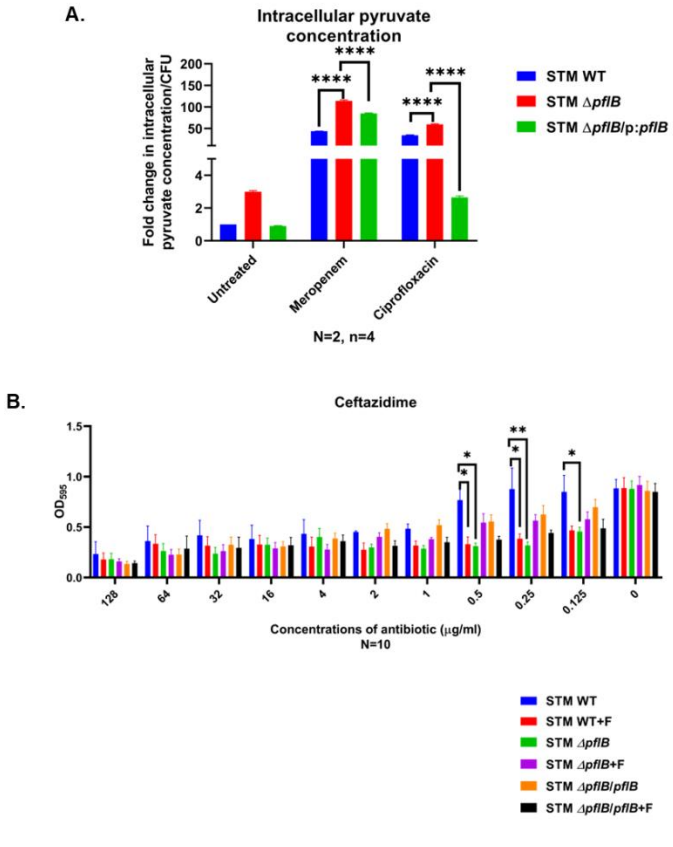

Figure S1

Figure S1: Deletion of *pflB* increased pyruvate levels in STM—a pattern also observed under antibiotic treatment—and additionally heightened STM's susceptibility to the third-generation cephalosporin ceftazidime, with a comparable sensitivity seen upon extracellular formate supplementation.

(A) Bar graphs showing fold change in intracellular pyruvate concentrations in STM WT, STM Δ*pflB*, STM Δ*pflB*/pQE60: *pflB* upon exposure to meropenem and ciprofloxacin. Data representative of N=2, n=4 and is presented as mean+/- SD.
(B) Ceftazidime susceptibility in STM WT, STM Δ*pflB*, and STM Δ*pflB*/pQE60: *pflB*, with or without formate, was evaluated using the microfold dilution method. Data is presented as mean+/-SEM of N=10.

(Unpaired two-tailed Student's t-test (column graphs), two-way ANOVA (grouped data), and

748 Mann–Whitney U-test (animal data).

749 (***p < 0.0001, **p < 0.001, **p < 0.01, *p < 0.05))

750

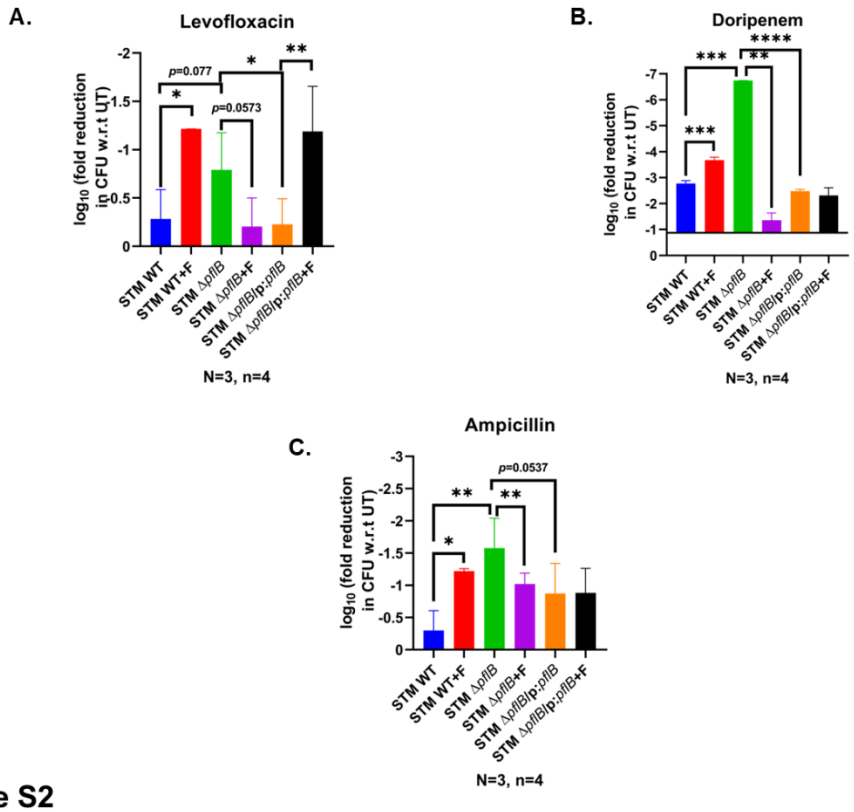

751 **Figure S2**

752 **Figure S2: Deletion of *pflB* increased STM susceptibility to the antibiotics levofloxacin,**
753 **doripenem, and ampicillin, and this effect was partially reversed by formate**
754 **supplementation. Formate addition to STM WT also heightened its sensitivity to these**
755 **antibiotics.**

756 Bar graphs show the $\log_{10}$ fold reduction in CFU relative to untreated controls for STM WT,
757 STM Δ*pflB*, and STM Δ*pflB*/pQE60: *pflB*, with or without formate, following exposure to
758 sub-lethal concentrations of levofloxacin (A), doripenem (B), and ampicillin (C).

759 Data representative of N=3, n=4 and is presented as mean+/- SD.

760 (Unpaired two-tailed Student's t-test (column graphs), two-way ANOVA (grouped data), and

761 Mann–Whitney U-test (animal data).

762 (***p < 0.0001, **p < 0.001, **p < 0.01, *p < 0.05))

763

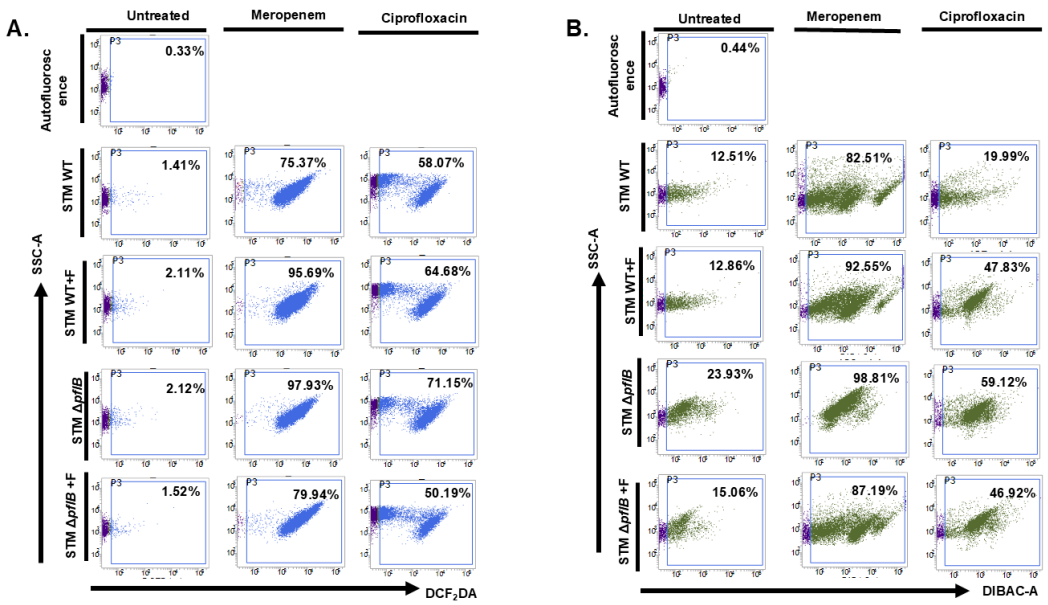

Figure S3

764

765 **Figure S3: Enhanced antibiotic sensitivity due to *pflB* deletion correlates with increased**

766 **DCF_2DA and DiBAC4 staining, indicating elevated ROS levels and membrane**

767 **depolarization—effects also seen in formate-treated STM WT.**

768 (A) Dot plots (SSC-A vs DCF_2DA) showing intracellular ROS following meropenem and

769 ciprofloxacin treatment in STM WT and STM Δ*pflB* with or without formate supplementation.

770 Data representative of N=3, n≥3.

771 (B) Dot plots (SSC-A vs DiBAC-A) showing membrane depolarization following meropenem

772 and ciprofloxacin treatment in STM WT and STM Δ*pflB* with or without formate

773 supplementation. Data representative of N=3, n≥3.

774 (Unpaired two-tailed Student's t-test (column graphs), two-way ANOVA (grouped data), and

775 Mann–Whitney U-test (animal data).

776 (***p < 0.0001, **p < 0.001, **p < 0.01, *p < 0.05))

777

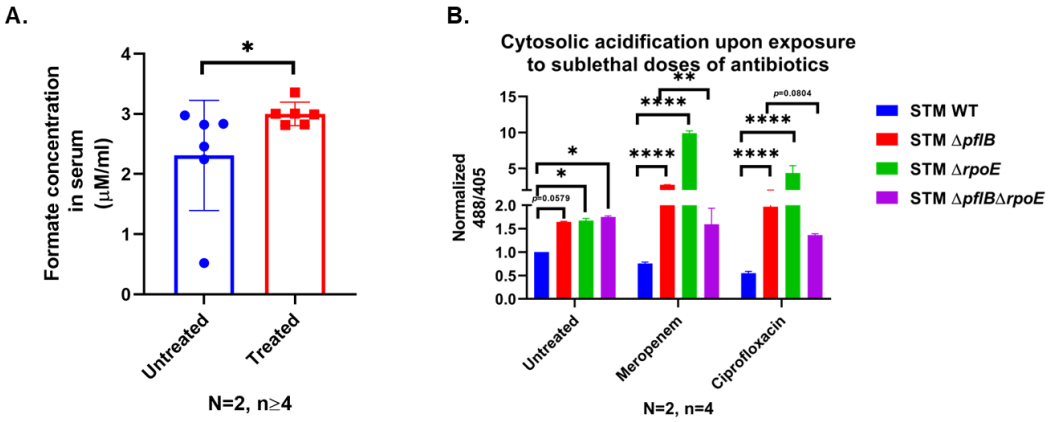

778 **Figure S4**

779 **Figure S4: Formate supplementation increased formate levels in serum of treated mice,**

780 **whereas *rpoE* deletion can also revert the enhanced ipH in STM Δ*pflB* in presence of**

781 **meropenem and ciprofloxacin.**

782 (A) Bar graph showing formate levels in mice serum after exposure to formate through drinking

783 water.

784 (B) Normalized 488/405 ratio of STM WT, STM Δ*pflB*, STM Δ*rpoE*, STM Δ*pflB*Δ*rpoE* in

785 presence of sub-lethal doses of meropenem and ciprofloxacin. Data representative of N=2, n=4

786 and is presented as mean+/- SD.

787

788 (Unpaired two-tailed Student's t-test (column graphs), two-way ANOVA (grouped data), and

789 Mann–Whitney U-test (animal data).

790 (***p < 0.0001, **p < 0.001, **p < 0.01, *p < 0.05))

791

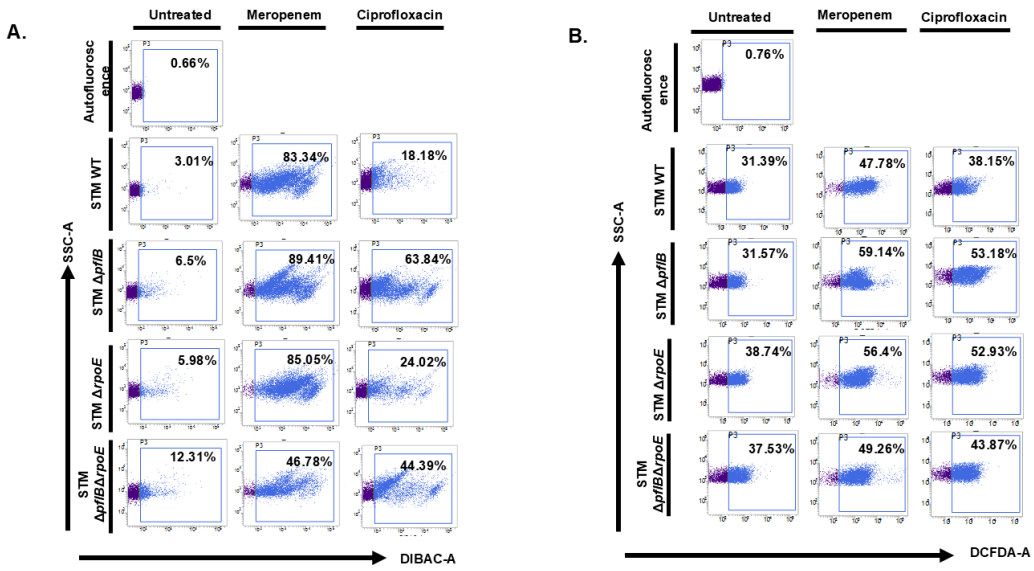

Figure S5

792

793 **Figure S5: Recovered antibiotic sensitivity due to *rpoE* deletion in STM Δ*pflB* correlates**

794 **with reduced intracellular ROS levels but it did not have any effect on membrane**

795 **depolarization**

796 (A) Representative dot plots (SSC-A vs. DIBAC-A) illustrating membrane depolarization in

797 STM WT, STM Δ*pflB*, STM Δ*rpoE,* STM Δ*pflB*Δ*rpoE* strains treated with meropenem or

798 ciprofloxacin. Data shown from three independent experiments (N=3, n=4).

799 (B) Representative dot plots (SSC-A vs. DCFDA-A) showing intracellular ROS in STM WT,

800 STM Δ*pflB*, STM Δ*rpoE,* STM Δ*pflB*Δ*rpoE* following treatment with meropenem or

801 ciprofloxacin. Data representative of N=3, n=4.

(Unpaired two-tailed Student's t-test (column graphs), two-way ANOVA (grouped data), and Mann–Whitney U-test (animal data).

(***p < 0.0001, **p < 0.001, **p < 0.01, *p < 0.05))

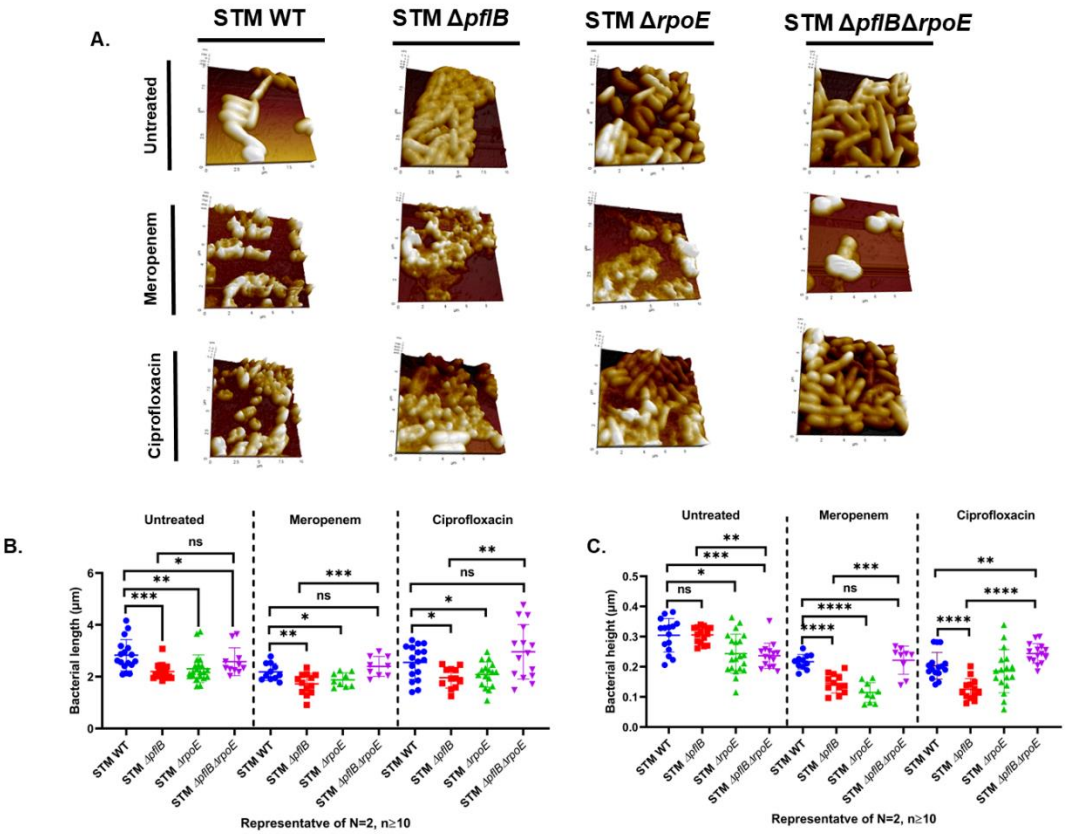

Figure S6

Figure S6: The recovery in antibiotic sensitivity upon *rpoE* deletion in STM Δ*pflB* was also evident from morphological changes under Atomic Force Microscopy

(A) AFM-assissted visualization of morphology of STM WT, STM Δ*pflB*, STM Δ*rpoE*, STM Δ*pflB*Δ*rpoE* upon expsure to sublethal concentrations of meropenem and ciprofloxacin.

(B-C) Quantification of bacterial length and height from the same.

(Unpaired two-tailed Student's t-test (column graphs), two-way ANOVA (grouped data), and Mann–Whitney U-test (animal data).

(***p < 0.0001, **p < 0.001, **p < 0.01, *p < 0.05))

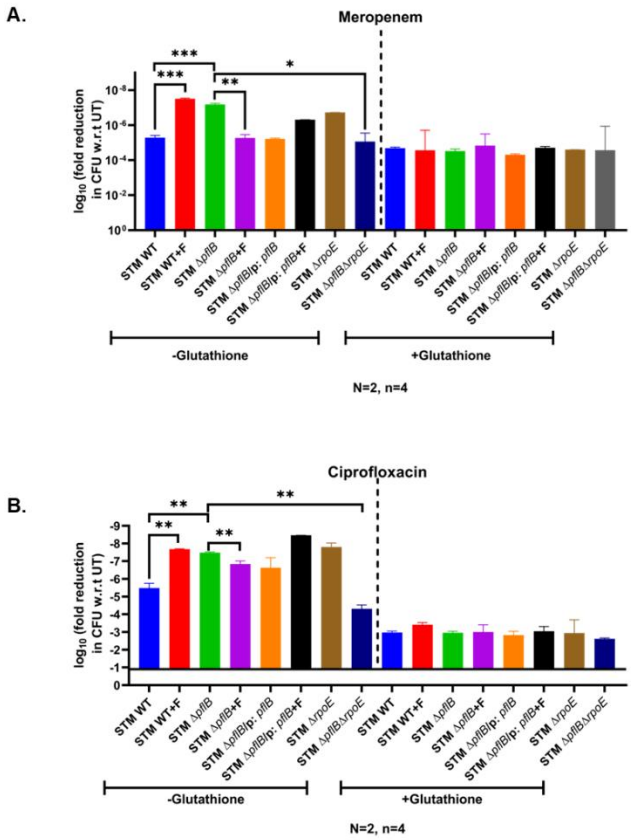

816 **Figure S7**

817 **Figure S7: Glutathione treatment equalizes the fold reduction in CFU observed in**
818 **meropenem- and ciprofloxacin-treated samples.**

819 (A-B) Bar graphs showing the $\log_{10}$ fold reduction in CFU relative to untreated controls (UT)
820 for STM WT (± formate), STM Δ*pflB* (± formate), STM Δ*pflB*/pQE60: *pflB* (± formate), STM
821 Δ*rpoE*, and STM Δ*pflB*Δ*rpoE* following meropenem or ciprofloxacin treatment, in the
822 presence or absence of glutathione. Data are presented as mean ± SD from two independent
823 experiments (N=2, n=4).

824 (Unpaired two-tailed Student's t-test (column graphs), two-way ANOVA (grouped data), and
825 Mann–Whitney U-test (animal data).

826 (***$p < 0.0001$, **$p < 0.001$, **$p < 0.01$, *$p < 0.05$))

827

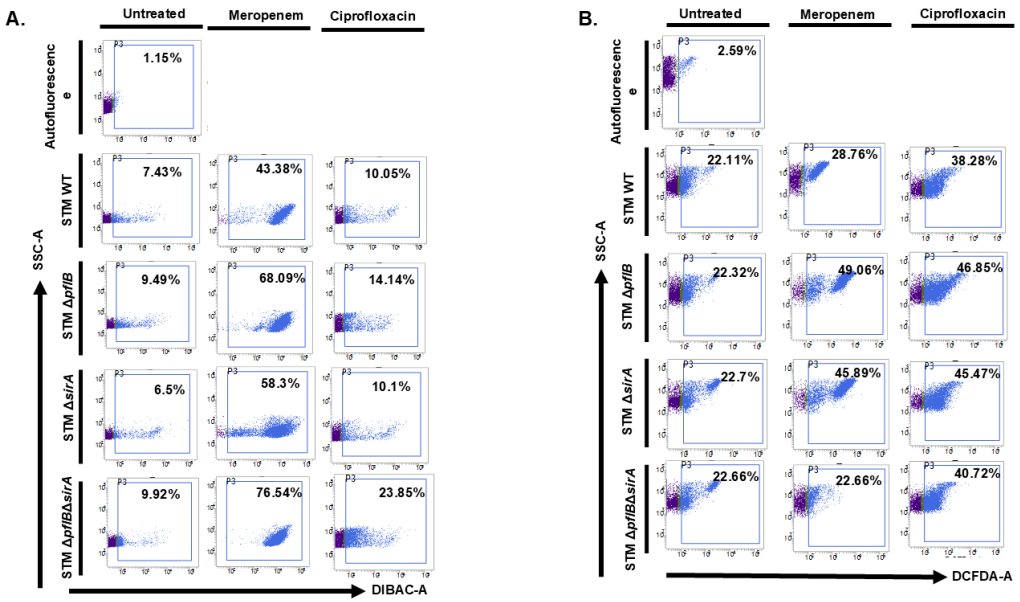

Figure S8

Figure S8: *sirA* deletion mediated reduction of antibiotic susceptibility in STM Δ*pflB* was associated with reduced intracellular ROS levels, but without any effect on membrane depolarization

(A) Representative dot plots (SSC-A vs. DiBAC4) depicting membrane depolarization in STM WT, STM Δ*pflB*, STM Δ*sirA*, and STM Δ*pflB*Δ*sirA* strains following treatment with meropenem or ciprofloxacin. Data shown from five independent experiments (N=5, n=3).

(B) Representative dot plots (SSC-A vs. DCFDA-A) showing intracellular ROS levels in STM WT, STM Δ*pflB*, STM Δ*sirA*, and STM Δ*pflB*Δ*sirA* following exposure to meropenem or ciprofloxacin. Data representative of N=5, n=3.

(Unpaired two-tailed Student's t-test (column graphs), two-way ANOVA (grouped data), and Mann–Whitney U-test (animal data).

(***$p < 0.0001$, **$p < 0.001$, **$p < 0.01$, *$p < 0.05$))

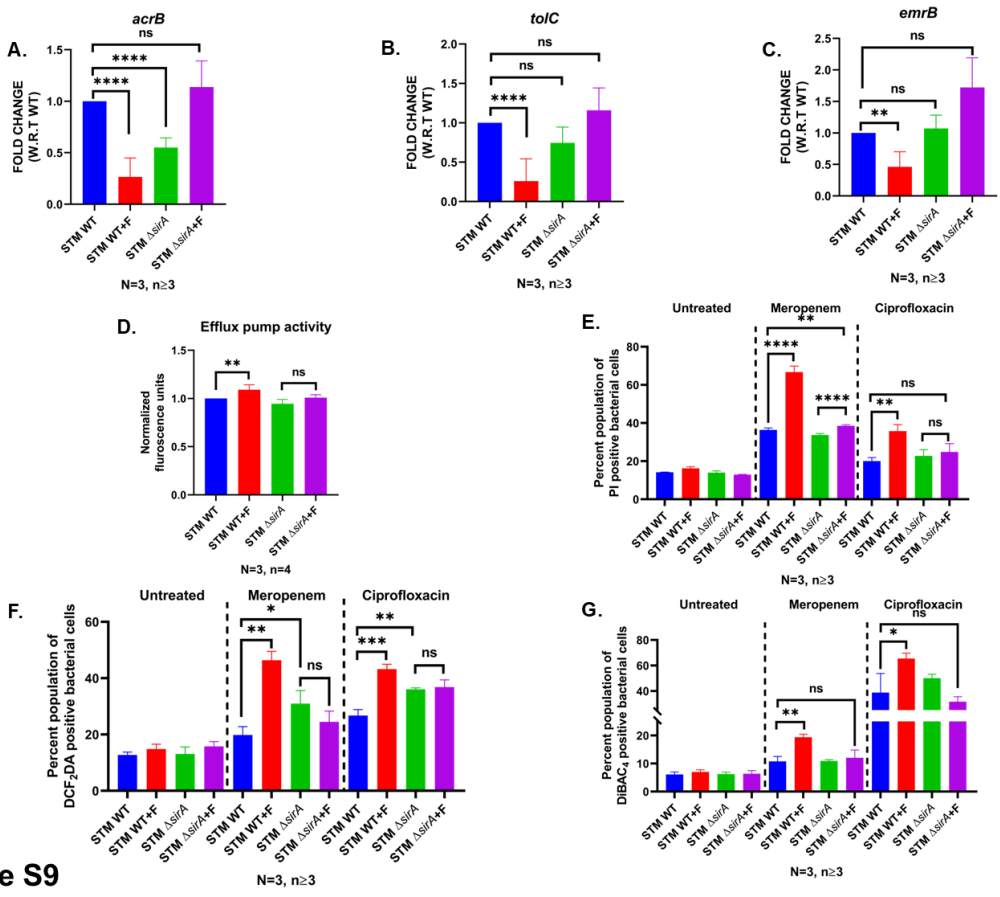

Figure S9

Figure S9: The deletion of *sirA* alleviates the heightened antibiotic sensitivity observed in STM WT upon external formate supplementation.

(A-C) RT-qPCR quantification of *acrB*, *tolC*, *emrB*, and *ompF* transcript levels in *STM WT* and STM Δ*sirA*, with or without formate supplementation. Data are presented as mean ± SD from N=3, n≥3.

(D) Quantification of PI-positive cells indicating bacterial death under antibiotic stress in STM WT and STM Δ*sirA*, with or without formate supplementation. Data are shown as mean ± SD from N=3, n≥3.

(E) Quantification of DCF_2DA-positive cells in STM WT and STM Δ*sirA* exposed to meropenem or ciprofloxacin, with or without formate supplementation. Representative data of N=3, n≥3 is presented as mean ± SD.

(F) Quantification of DiBAC4-positive cells in STM WT and STM Δ*sirA*, with or without formate, reflecting membrane depolarization under antibiotic stress. Representative data of N=3, n≥3 is presented as mean ± SD.

(Unpaired two-tailed Student's t-test (column graphs), two-way ANOVA (grouped data), and Mann–Whitney U-test (animal data).

(***$p < 0.0001$, **$p < 0.001$, **$p < 0.01$, *$p < 0.05$))

Graphical abstract: Graphical abstract showing regulation of AMR in *Salmonella* by formate

References:

1. Zhu S, Yang B, Jia Y, Yu F, Wang Z, Liu Y. Comprehensive analysis of disinfectants on the horizontal transfer of antibiotic resistance genes. J Hazard Mater. 2023;453:131428.
2. Brauner A, Fridman O, Gefen O, Balaban NQ. Distinguishing between resistance, tolerance and persistence to antibiotic treatment. Nat Rev Microbiol. 2016;14(5):320-30.
3. Antimicrobial Resistance C. Global burden of bacterial antimicrobial resistance in 2019: a systematic analysis. Lancet. 2022;399(10325):629-55.
4. Azmatullah A, Qamar FN, Thaver D, Zaidi AK, Bhutta ZA. Systematic review of the global epidemiology, clinical and laboratory profile of enteric fever. J Glob Health. 2015;5(2):020407.
5. Kim TH, Hwang HJ, Kim JH. Development of a Novel, Rapid Multiplex Polymerase Chain Reaction Assay for the Detection and Differentiation of Salmonella enterica Serovars Enteritidis and Typhimurium Using Ultra-Fast Convection Polymerase Chain Reaction. Foodborne Pathog Dis. 2017;14(10):580-6.
6. Zhang H, Yao S, Sheng R, Wang J, Li H, Fu Y, et al. A cascade amplification strategy for ultrasensitive Salmonella typhimurium detection based on DNA walker coupling with CRISPR-Cas12a. J Colloid Interface Sci. 2022;625:257-63.
7. Wu S, Ji J, Sheng L, Ye Y, Zhang Y, Sun X. Lysine and valine weaken antibiotic resistance in Salmonella Typhimurium induced by disinfectant stress. J Hazard Mater. 2024;480:135858.
8. Punchihewage-Don AJ, Ranaweera PN, Parveen S. Defense mechanisms of Salmonella against antibiotics: a review. Front Antibiot. 2024;3:1448796.
9. Chowdhury AR, Mukherjee D, Chatterjee R, Chakravortty D. Defying the odds: Determinants of the antimicrobial response of Salmonella Typhi and their interplay. Mol Microbiol. 2024;121(2):213-29.
10. Mukherjee D, Noor S, Mukherjee T, Singh M, Chakravortty D. Intracellular formate modulates a motility-invasion switch in Salmonella Typhimurium. PLoS Pathog. 2025;21(9):e1013453.
11. Lyu Z, Yang A, Villanueva P, Singh A, Ling J. Heterogeneous Flagellar Expression in Single Salmonella Cells Promotes Diversity in Antibiotic Tolerance. mBio. 2021;12(5):e0237421.

12. Chowdhury AR, Mukherjee D, Singh AK, Chakravortty D. Loss of outer membrane protein A (OmpA) impairs the survival of Salmonella Typhimurium by inducing membrane damage in the presence of ceftazidime and meropenem. J Antimicrob Chemother. 2022;77(12):3376-89.
13. Hughes ER, Winter MG, Duerkop BA, Spiga L, Furtado de Carvalho T, Zhu W, et al. Microbial Respiration and Formate Oxidation as Metabolic Signatures of Inflammation-Associated Dysbiosis. Cell Host Microbe. 2017;21(2):208-19.
14. Drescher SPM, Gallo SW, Ferreira PMA, Ferreira CAS, Oliveira SD. Salmonella enterica persister cells form unstable small colony variants after in vitro exposure to ciprofloxacin. Sci Rep. 2019;9(1):7232.
15. Reyes-Fernandez EZ, Schuldiner S. Acidification of Cytoplasm in Escherichia coli Provides a Strategy to Cope with Stress and Facilitates Development of Antibiotic Resistance. Sci Rep. 2020;10(1):9954.
16. Panta PR, Doerrler WT. A link between pH homeostasis and colistin resistance in bacteria. Sci Rep. 2021;11(1):13230.
17. Huang Y, Suyemoto M, Garner CD, Cicconi KM, Altier C. Formate acts as a diffusible signal to induce Salmonella invasion. J Bacteriol. 2008;190(12):4233-41.
18. Papich MG. Saunders handbook of veterinary drugs. North Carolina. 2016;12:162-71.
19. El-Saeed BA, Elshebrawy HA, Zakaria AI, Abdelkhalek A, Sallam KI. Colistin-, cefepime-, and levofloxacin-resistant Salmonella enterica serovars isolated from Egyptian chicken carcasses. Ann Clin Microbiol Antimicrob. 2024;23(1):61.
20. Tang HJ, Chen CC, Zhang CC, Cheng KC, Chiang SR, Chiu YH, et al. Use of Carbapenems against clinical, nontyphoid Salmonella isolates: results from in vitro and in vivo animal studies. Antimicrob Agents Chemother. 2012;56(6):2916-22.
21. Chang HR, Vladoianu IR, Pechere JC. Effects of ampicillin, ceftriaxone, chloramphenicol, pefloxacin and trimethoprim-sulphamethoxazole on Salmonella typhi within human monocyte-derived macrophages. J Antimicrob Chemother. 1990;26(5):689-94.
22. Dwyer DJ, Kohanski MA, Hayete B, Collins JJ. Gyrase inhibitors induce an oxidative damage cellular death pathway in Escherichia coli. Mol Syst Biol. 2007;3:91.
23. Kohanski MA, Dwyer DJ, Hayete B, Lawrence CA, Collins JJ. A common mechanism of cellular death induced by bactericidal antibiotics. Cell. 2007;130(5):797-810.
24. Dwyer DJ, Belenky PA, Yang JH, MacDonald IC, Martell JD, Takahashi N, et al. Antibiotics induce redox-related physiological alterations as part of their lethality. Proc Natl Acad Sci U S A. 2014;111(20):E2100-9.
25. May KL, Grabowicz M. The bacterial outer membrane is an evolving antibiotic barrier. Proc Natl Acad Sci U S A. 2018;115(36):8852-4.
26. Epand RF, Pollard JE, Wright JO, Savage PB, Epand RM. Depolarization, bacterial membrane composition, and the antimicrobial action of ceragenins. Antimicrob Agents Chemother. 2010;54(9):3708-13.
27. Te Winkel JD, Gray DA, Seistrup KH, Hamoen LW, Strahl H. Analysis of Antimicrobial-Triggered Membrane Depolarization Using Voltage Sensitive Dyes. Front Cell Dev Biol. 2016;4:29.
28. Han FF, Gao YH, Luan C, Xie YG, Liu YF, Wang YZ. Comparing bacterial membrane interactions and antimicrobial activity of porcine lactoferricin-derived peptides. J Dairy Sci. 2013;96(6):3471-87.
29. Soren O, Brinch KS, Patel D, Liu Y, Liu A, Coates A, et al. Antimicrobial Peptide Novicidin Synergizes with Rifampin, Ceftriaxone, and Ceftazidime against Antibiotic-Resistant Enterobacteriaceae In Vitro. Antimicrob Agents Chemother. 2015;59(10):6233-40.
30. Cheng M, Huang JX, Ramu S, Butler MS, Cooper MA. Ramoplanin at bactericidal concentrations induces bacterial membrane depolarization in Staphylococcus aureus. Antimicrob Agents Chemother. 2014;58(11):6819-27.
31. Masi M, Refregiers M, Pos KM, Pages JM. Mechanisms of envelope permeability and antibiotic influx and efflux in Gram-negative bacteria. Nat Microbiol. 2017;2:17001.

32. Du D, Wang-Kan X, Neuberger A, van Veen HW, Pos KM, Piddock LJV, et al. Multidrug efflux pumps: structure, function and regulation. Nat Rev Microbiol. 2018;16(9):523-39.
33. Ramaswamy VK, Vargiu AV, Malloci G, Dreier J, Ruggerone P. Molecular Rationale behind the Differential Substrate Specificity of Bacterial RND Multi-Drug Transporters. Sci Rep. 2017;7(1):8075.
34. Rosenberg EY, Ma D, Nikaido H. AcrD of Escherichia coli is an aminoglycoside efflux pump. J Bacteriol. 2000;182(6):1754-6.
35. Webber MA, Bailey AM, Blair JM, Morgan E, Stevens MP, Hinton JC, et al. The global consequence of disruption of the AcrAB-TolC efflux pump in Salmonella enterica includes reduced expression of SPI-1 and other attributes required to infect the host. J Bacteriol. 2009;191(13):4276-85.
36. Ziervogel BK, Roux B. The binding of antibiotics in OmpF porin. Structure. 2013;21(1):76-87.
37. Choi KM, Kim MH, Cai H, Lee YJ, Hong Y, Ryu PY. Salicylic Acid Reduces OmpF Expression, Rendering Salmonella enterica Serovar Typhimurium More Resistant to Cephalosporin Antibiotics. Chonnam Med J. 2018;54(1):17-23.
38. Roy Chowdhury A, Sah S, Varshney U, Chakravortty D. Salmonella Typhimurium outer membrane protein A (OmpA) renders protection from nitrosative stress of macrophages by maintaining the stability of bacterial outer membrane. PLoS Pathog. 2022;18(8):e1010708.
39. Dhayade S, Pietzke M, Wiesheu R, Tait-Mulder J, Athineos D, Sumpton D, et al. Impact of Formate Supplementation on Body Weight and Plasma Amino Acids. Nutrients. 2020;12(8).
40. Hayden JD, Ades SE. The extracytoplasmic stress factor, sigmaE, is required to maintain cell envelope integrity in Escherichia coli. PLoS One. 2008;3(2):e1573.
41. Ahuja N, Korkin D, Chaba R, Cezairliyan BO, Sauer RT, Kim KK, et al. Analyzing the interaction of RseA and RseB, the two negative regulators of the sigmaE envelope stress response, using a combined bioinformatic and experimental strategy. J Biol Chem. 2009;284(8):5403-13.
42. Lima S, Guo MS, Chaba R, Gross CA, Sauer RT. Dual molecular signals mediate the bacterial response to outer-membrane stress. Science. 2013;340(6134):837-41.
43. De Las Penas A, Connolly L, Gross CA. The sigmaE-mediated response to extracytoplasmic stress in Escherichia coli is transduced by RseA and RseB, two negative regulators of sigmaE. Mol Microbiol. 1997;24(2):373-85.
44. Missiakas D, Mayer MP, Lemaire M, Georgopoulos C, Raina S. Modulation of the Escherichia coli sigmaE (RpoE) heat-shock transcription-factor activity by the RseA, RseB and RseC proteins. Mol Microbiol. 1997;24(2):355-71.
45. Campbell EA, Tupy JL, Gruber TM, Wang S, Sharp MM, Gross CA, et al. Crystal structure of Escherichia coli sigmaE with the cytoplasmic domain of its anti-sigma RseA. Mol Cell. 2003;11(4):1067-78.
46. Pannuri A, Vakulskas CA, Zere T, McGibbon LC, Edwards AN, Georgellis D, et al. Circuitry Linking the Catabolite Repression and Csr Global Regulatory Systems of Escherichia coli. J Bacteriol. 2016;198(21):3000-15.
47. Yakhnin H, Aichele R, Ades SE, Romeo T, Babitzke P. Circuitry Linking the Global Csr- and sigma(E)-Dependent Cell Envelope Stress Response Systems. J Bacteriol. 2017;199(23).
48. Ricci V, Attah V, Overton T, Grainger DC, Piddock LJV. CsrA maximizes expression of the AcrAB multidrug resistance transporter. Nucleic Acids Res. 2017;45(22):12798-807.
49. Gu Y, Huang L, Wu C, Huang J, Hao H, Yuan Z, et al. The Evolution of Fluoroquinolone Resistance in Salmonella under Exposure to Sub-Inhibitory Concentration of Enrofloxacin. Int J Mol Sci. 2021;22(22).
50. Parmar K, Kumari Y, Rajmani RS, Chakravortty D. The resilience of Salmonella to bile stress is impaired due to the reduced efflux pump activity mediated by the antioxidant enzyme YqhD. bioRxiv. 2024:2024.11.23.625033.

51. Salvail H, Groisman EA. The phosphorelay BarA/SirA activates the non-cognate regulator RcsB in Salmonella enterica. PLoS Genet. 2020;16(5):e1008722.
52. Nava-Galeana J, Nunez C, Bustamante VH. Proteomic analysis reveals the global effect of the BarA/SirA-Csr regulatory cascade in Salmonella Typhimurium grown in conditions that favor the expression of invasion genes. J Proteomics. 2023;286:104960.
53. Gudapaty S, Suzuki K, Wang X, Babitzke P, Romeo T. Regulatory interactions of Csr components: the RNA binding protein CsrA activates csrB transcription in Escherichia coli. J Bacteriol. 2001;183(20):6017-27.
54. Martinez LC, Yakhnin H, Camacho MI, Georgellis D, Babitzke P, Puente JL, et al. Integration of a complex regulatory cascade involving the SirA/BarA and Csr global regulatory systems that controls expression of the Salmonella SPI-1 and SPI-2 virulence regulons through HilD. Mol Microbiol. 2011;80(6):1637-56.
55. Huemer M, Mairpady Shambat S, Brugger SD, Zinkernagel AS. Antibiotic resistance and persistence-Implications for human health and treatment perspectives. EMBO Rep. 2020;21(12):e51034.
56. Algarni S, Ricke SC, Foley SL, Han J. The Dynamics of the Antimicrobial Resistance Mobilome of Salmonella enterica and Related Enteric Bacteria. Front Microbiol. 2022;13:859854.
57. Dyson ZA, Klemm EJ, Palmer S, Dougan G. Antibiotic Resistance and Typhoid. Clin Infect Dis. 2019;68(Suppl 2):S165-S70.
58. Wu S, Yang Y, Wang T, Sun J, Zhang Y, Ji J, et al. Effects of acid, alkaline, cold, and heat environmental stresses on the antibiotic resistance of the Salmonella enterica serovar Typhimurium. Food Research International. 2021;144:110359.
59. Kuang X, Hao H, Dai M, Wang Y, Ahmad I, Liu Z, et al. Serotypes and antimicrobial susceptibility of Salmonella spp. isolated from farm animals in China. Front Microbiol. 2015;6:602.
60. Kebede A, Kemal J, Alemayehu H, Habte Mariam S. Isolation, Identification, and Antibiotic Susceptibility Testing of Salmonella from Slaughtered Bovines and Ovines in Addis Ababa Abattoir Enterprise, Ethiopia: A Cross-Sectional Study. Int J Bacteriol. 2016;2016:3714785.
61. Christou A, Aguera A, Bayona JM, Cytryn E, Fotopoulos V, Lambropoulou D, et al. The potential implications of reclaimed wastewater reuse for irrigation on the agricultural environment: The knowns and unknowns of the fate of antibiotics and antibiotic resistant bacteria and resistance genes - A review. Water Res. 2017;123:448-67.
62. Sunuwar J, Azad RK. A machine learning framework to predict antibiotic resistance traits and yet unknown genes underlying resistance to specific antibiotics in bacterial strains. Brief Bioinform. 2021;22(6).
63. Devanga Ragupathi NK, Muthuirulandi Sethuvel DP, Shankar BA, Munusamy E, Anandan S, Veeraraghavan B. Draft genome sequence of bla(TEM-1)-mediated cephalosporin-resistant Salmonella enterica serovar Typhi from bloodstream infection. J Glob Antimicrob Resist. 2016;7:11-2.
64. Greninger AL, Chatterjee SS, Chan LC, Hamilton SM, Chambers HF, Chiu CY. Whole-Genome Sequencing of Methicillin-Resistant Staphylococcus aureus Resistant to Fifth-Generation Cephalosporins Reveals Potential Non-mecA Mechanisms of Resistance. PLoS One. 2016;11(2):e0149541.
65. Palzkill T. Structural and Mechanistic Basis for Extended-Spectrum Drug-Resistance Mutations in Altering the Specificity of TEM, CTX-M, and KPC beta-lactamases. Front Mol Biosci. 2018;5:16.
66. Sanders CC. beta-Lactamase stability and in vitro activity of oral cephalosporins against strains possessing well-characterized mechanisms of resistance. Antimicrob Agents Chemother. 1989;33(8):1313-7.

67. Ji J, Wu S, Sheng L, Sun J, Ye Y, Zhang Y, et al. Metabolic reprogramming of the glutathione biosynthesis modulates the resistance of Salmonella Derby to ceftriaxone. iScience. 2023;26(8):107263.
68. Wu S, Ji J, Carole NVD, Yang J, Yang Y, Sun J, et al. Combined metabolomics and transcriptomics analysis reveals the mechanism of antibiotic resistance of Salmonella enterica serovar Typhimurium after acidic stress. Food Microbiol. 2023;115:104328.
69. Teplitski M, Goodier RI, Ahmer BM. Pathways leading from BarA/SirA to motility and virulence gene expression in Salmonella. J Bacteriol. 2003;185(24):7257-65.
70. Kitzenberg DA, Lee JS, Mills KB, Kim JS, Liu L, Vazquez-Torres A, et al. Adenosine Awakens Metabolism to Enhance Growth-Independent Killing of Tolerant and Persister Bacteria across Multiple Classes of Antibiotics. mBio. 2022;13(3):e0048022.